Earth-like Habitable Environments in the Subsurface of Mars

J.D. D Tarnas, J.F. F Mustard, B. Sherwood Lollar, V. Stamenković, K.M. M Cannon, J.-P. Lorand, T.C. C Onstott, J.R. R Michalski, O. Warr, A.M. M Palumbo, et al.

Earth-like habitable environments in the subsurface of Mars

J.D. Tarnas[1], J.F. Mustard[1], B. Sherwood Lollar[2], V. Stamenković[3], K.M. Cannon[4,5], J.-P. Lorand[6], T.C. Onstott[7], J.R. Michalski[8], O. Warr[2], A.M. Palumbo[1], A.-C. Plesa[9]

[1]Brown University Department of Earth, Environmental and Planetary Sciences, [2]University of Toronto Department of Earth Sciences, [3]NASA Jet Propulsion Laboratory, California Institute of Technology, [4]Department of Geology and Geological Engineering, Colorado School of Mines, [5]Space Resources Program, Colorado School of Mines, [6]Université de Nantes Laboratoire de Planétologie et Géodynamique de Nantes, [7]Princeton University Department of Geosciences, [8]University of Hong Kong Division of Earth & Planetary Science, [9]German Aerospace Center (DLR) Institute of Planetary Research

Abstract

In Earth's deep continental subsurface, where groundwaters are often isolated for $>10^6$-10^9 years, energy released by radionuclides within rock produces oxidants and reductants that drive metabolisms of non-photosynthetic microorganisms. Similar processes could support past and present life in the martian subsurface. Sulfate-reducing microorganisms are common in Earth's deep subsurface, often using hydrogen derived directly from radiolysis of pore water and sulfate derived from oxidation of rock-matrix-hosted sulfides by radiolytically-derived oxidants. Radiolysis thus produces redox energy to support a deep biosphere in groundwaters isolated from surface substrate input for millions to billions of years on Earth. Here we demonstrate that radiolysis by itself could produce sufficient redox energy to sustain a habitable environment in

the subsurface of present-day Mars, one in which Earth-like microorganisms could survive wherever groundwater exists. We show that the source localities for many martian meteorites are capable of producing sufficient redox nutrients to sustain up to millions of sulfate-reducing microbial cells per kg rock via radiolysis alone, comparable to cell densities observed in many regions of Earth's deep subsurface. Additionally, we calculate variability in supportable sulfate-reducing cell densities between the martian meteorite source regions. Our results demonstrate that martian subsurface groundwaters, where present, would largely be habitable by sulfate-reducing bacteria from a redox energy perspective via radiolysis alone.

1.0 Introduction

The surface of Mars is an extremely hostile environment characterized by freezing temperatures, desiccating conditions, high levels of ionizing radiation, oxidizing chemicals, low pressures, and a lack of liquid water that preclude any Earth-like organisms from surviving without adaptation that is unprecedented on Earth. Though some extremophiles on Earth have evolved to tolerate certain conditions relevant for Mars, any martian life formed in earlier eras would have taken refuge in the subsurface for survival (National Academies of Sciences, Engineering, and Medicine et al., 2018; Michalski et al., 2018), perhaps temporarily inhabiting transiently habitable near-surface environments formed by meteorite impacts into ice-rich rock (Schwenzer et al., 2012). Within the last three decades, researchers have discovered that fluids preserved within Earth's kilometers deep subsurface contain significant quantities of biomass utilizing a wide diversity of redox reactions to drive their microbial metabolisms (Onstott et al., 2019). Similar habitable subsurface environments could potentially have existed on ancient Mars (Onstott et al., 2019; Tarnas et al., 2018), may still exist on modern Mars (Michalski et al.,

2013), and could exist on other planetary objects including ocean worlds, small bodies like Ceres, and exoplanets, making them an exciting frontier of planetary exploration (National Academies of Sciences, Engineering, and Medicine et al., 2018; Stamenković et al., 2019). Planetary objects with lower surface gravity than Earth, including Mars, likely have higher volumes of habitable pore and fracture space that extend deeper into the crust compared to Earth (e.g., Goossens et al., 2017; Lewis et al., 2019), increasing the volume of feasibly supportable biomass if sufficient liquid water and redox energy is available (Sleep, 2012).

In Earth's subsurface, actively metabolizing microbes can be sustained by fluids that have been isolated from surface substrate input for $>10^6$-10^9 years (Lin et al., 2006; Holland et al., 2013; Li et al., 2016; Warr et al., 2018; Lollar et al., 2019)—similar to groundwater isolation timescales expected on Mars (Grimm et al., 2017)—powered solely by redox energy derived from water-rock reactions including radiolysis and serpentinization (Sherwood Lollar et al., 2014; Warr et al., 2019). Radiolysis, the breaking of H_2O molecules in pore spaces by α, β, and ɣ radiation released from decay of radionuclides within host rock, generates both dissolved reductants (e.g. H_2; Lin et al., 2005b; Warr et al., 2019) and dissolved oxidants (e.g. H_2O_2; ref. Lefticariu et al., 2010; Li et al., 2016). The dissolved H_2 generated by radiolysis can be used directly as a reductant by subsurface microbes, while the primary oxidant byproducts of radiolysis can oxidize sulfides within the host rock matrix to form dissolved sulfate (SO_4) (Lefticariu et al., 2010; Li et al., 2016) that can then be used by microbes as an oxidant (Lin et al., 2005b; Lin et al., 2006; Chivian et al., 2008; Li et al., 2016; Lollar et al., 2019). Sulfate-reducing microorganisms are found kilometers deep on Earth in many groundwaters that have been isolated for $>10^7$ years (Lin et al., 2005b; Lin et al., 2006; Chivian et al., 2008; Li et al., 2016; Lollar et al., 2019), and a significant component of the H_2 and SO_4 in especially ancient

groundwaters is typically derived from radiolysis (Li et al., 2016; Warr et al., 2019). Radiation doses from decay of rock-matrix-hosted radionuclides are insufficient to sterilize microbial communities, as demonstrated by the presence of microbes in these subsurface settings (e.g., Lin et al., 2005a; Lin et al. 2005b; Lin et al. 2006; Chivian et al., 2008; Lollar et al., 2019). Thus, these Earth systems prove that in any subsurface environment containing radionuclides, liquid H_2O, and sulfides, radiolysis alone has the potential to provide sufficient biologically-supportive redox energy to sustain a subsurface biome (Onstott et al., 2006; Sherwood Lollar et al., 2014). There are many alternative potential pathways to generate additional redox couples for life in subsurface martian environments, including in fluid mixing zones that create chemical disequilibria (Sherwood Lollar et al., 2007), which will not be considered here. Accordingly, the gas production rates and supportable cell density ranges presented in this work should be considered conservative estimates.

2.0 Methods

2.1 Summary

The model used to estimate H_2 production rates, sulfate production rates, dissolved H_2 concentrations, dissolved sulfate concentrations, and supportable sulfate-reducing cell densities is similar to models employed in Lefticariu et al., (2010); Li et al., (2016); and Altair et al., (2018) (Section 2.2). Porosity (Section 2.3), sulfide concentrations (Section 2.4), average sulfide grain sizes (Section 2.5), radionuclide concentrations (Section 2.6), and sulfate-reducing metabolic rates are the key parameters necessary to constrain the model. H_2 production rates are dependent on porosity and radionuclide concentrations, increasing as porosity and radionuclide concentrations increase. Sulfate production rates are dependent on porosity, radionuclide

93 concentrations, sulfide concentrations, and average sulfide grain size. They increase as porosity,
94 radionuclide concentrations, and sulfide concentrations increase and decrease as sulfide grain
95 size increases, as less reactive surface area is exposed when sulfide grains are larger. Dissolved
96 H_2 and sulfate concentrations increase as porosity decreases, as there is less fluid in which to
97 dissolve the H_2 and sulfate that is produced. Supportable sulfate-reducing cell densities in units
98 of cells $(kg\ rock)^{-1}$ increase as porosity and sulfate production rates increase, since sulfate is the
99 limiting redox nutrient in all model results presented here. Supportable sulfate-reducing cell
100 densities in units of cells L^{-1} decrease as porosity increases because there is less fluid per volume
101 rock for the cells to reside in. Supportable sulfate-reducing cell densities are higher when the
102 assumed sulfate-reducing metabolic rate is lower.

103 Porosity is constrained using density estimates for the martian crust from orbital
104 gravimetry (Goossens et al., 2017) that are supported by rover gravimetry (Lewis et al., 2019)
105 (Section 2.3). Sulfide concentrations (Section 2.4), average sulfide grain sizes (Section 2.5), and
106 radionuclide concentrations (Section 2.6) are constrained by their measured values in martian
107 meteorites. The maximum and minimum assumed sulfate-reducing metabolic rates are based on
108 the fastest and slowest sulfate-reducing metabolic rates estimated for fracture fluids in the gold
109 mines of the Witwatersrand Basin (Lin et al., 2006; Chivian et al., 2008). The calculated sulfate-
110 reducing cell densities are compared to those found in Earth's deep subsurface (Onstott et al.,
111 2003; Cockell et al., 2012; Magnabosco et al., 2018; Onstott et al., 2019) (Fig. 2).

112 The amount of radiolytic hydrogen and sulfate that would be produced in each of the
113 different martian meteorite source regions is calculated based on their individual K, Th, and U
114 concentrations (Fig. 1e, Table 2), sulfide concentrations (Fig. 1f, Table 1), average sulfide grain
115 sizes (Fig. 1f, Table 1), and estimated range of porosity (Fig. 1c, Table 2) before the impact

events that ejected these rocks from the martian gravity well. Based on the produced amounts of these redox nutrients, the number of supportable sulfate-reducing cells per kg rock is calculated for each of these meteorite source regions using the range of sulfate-reducing metabolic rates observed in Earth's deep subsurface (Lin et al., 2006; Chivian et al., 2008). Porosity range assumptions are based on density estimates of different martian terrains from orbital gravimetry (Fig. 1c-d; Section 2.2) (Goossens et al., 2017), a range that is supported by rover gravimetry (Lewis et al., 2019). The radiolysis model applied here (Section 2.3) is similar to the one employed in Lin et al., (2005b); Li et al., (2016); Dzaugis et al., (2018); Tarnas et al., (2018); and Warr et al., (2019).

2.2 Radiolysis model

The model used here follows the radiolytic H_2 and SO_4 production models presented in Lin et al., (2005a); Lin et al., (2005b); Li et al., (2016); Tarnas et al., (2018); and Warr et al., (2019). This calculates radiogenic dose rate as

$$(1)\ E_{net,i} = \frac{E_i \times W \times S_i}{1+W \times S_i}$$

where i is α, β, or γ radiation, E_{net} is the net dosage absorbed by pore water (eV kg^{-1} s^{-1}), E is the apparent dosage from radioactive element decay (eV kg^{-1} s^{-1}), W is the weight ratio of pore water to rock, and S is the stopping power of minerals within the rock matrix with respect to each type of radiation particle/ray, where S_α = 1.5, $S_\beta = 1.25$, $S_\gamma = 1.14$ (Lin et al., 2005a; Lin et al., 2005b; Tarnas et al., 2018; Warr et al., 2019). The stopping power of minerals can be estimated using Bragg's law (Bragg and Kleeman, 1905) and typically varies by <0.5 for silicate minerals (Nogami and Hurley, 1948).

W, the weight ratio of pore water to rock, primarily depends on the rock porosity with additional minor variations induced by differences in water density in solid (~900 kg m^{-3}) or liquid (~1000 kg m^{-3}) phase. Values from Adamiec and Aitken, 1998 are used for E for 1 wt. % K, 1 ppm Th, and 1 ppm U for α, β, and γ radiation, which are $E_{K,\alpha}$ = 0 (Gy ka^{-1}), $E_{K,\beta}$ = 0.782 (Gy ka^{-1}), $E_{K,\gamma} = 0.243$ (Gy ka^{-1}), $E_{Th,\alpha} = 0.061$ (Gy ka^{-1}), $E_{Th,\beta} = 0.027$ (Gy ka^{-1}), $E_{Th,\gamma} = 0.048$ (Gy ka^{-1}), $E_{U,\alpha} = 0.218$ (Gy ka^{-1}), $E_{U,\beta} = 0.146$ (Gy ka^{-1}), $E_{U,\gamma} = 0.113$ (Gy ka^{-1}). 1 Gy = 6.2415×10^{18} eV kg^{-1}.

H_2 yield is calculated as

$$(2)\ Y_{H2} = \sum E_{net,i} \times G_{H2,i}$$

where Y_{H2} is the total yield of H_2 molecules (molecules kg^{-1} s^{-1}) and G_{H2} is the number of H_2 molecules produced per 100 eV of radiation. The conversion factor between (kg water) and (kg water and rock matrix) is W, the weight ratio of pore water to rock. For H_2O, $G_{H2,\alpha} = 0.96$ H_2 molecules $(100\ eV)^{-1}$, $G_{H2,\beta} = 0.6$ H_2 molecules $(100\ eV)^{-1}$, $G_{H2,\gamma} = 0.4$ H_2 molecules $(100\ eV)^{-1}$ (Lin et al., 2005a; Lin et al., 2005b; Tarnas et al., 2018; Warr et al., 2019). The value of G_{H2} changes depending on the liquid or solid substance filling the pore space, and has received extensive study due to its importance in the context of nuclear waste storage. It is typically higher for chloride brines than for pure water (LaVerne and Tandon, 2005; Buck et al., 2012) due to the reaction of dissolved brine ions (e.g. Cl^-) with ions formed via radiative destruction of neutral H_2O molecules (e.g. OH·). This causes a depletion of ions that would react with H· generated by radiolysis, leaving more H· in solution, which reacts to form H_2 (2H· → H_2) (Klein et al., 2020) . Hydrated chloride salts, embedded in either pore space or within the rock matrix, will also produce H_2, though at lower production efficiencies relative to pure water, ice, or brine (LaVerne and Tandon, 2005). These different production efficiencies are summarized in Tarnas

et al., 2018 and references therein. Presence of certain minerals, such as zeolites, can significantly increase H_2 and oxidant production efficiency from radiolysis (Kumagai et al., 2013). Zeolites are found in both bedrock (Ehlmann et al., 2009) and dust (Ruff, 2004) on Mars, thus this mineral is expected to enhance radiolytic H_2 and oxidant production in some parts of the crust, but this effect is not modeled here in order to focus on the most conservative estimates possible.

SO_4 production is calculated as

$$(3)\ Y_{SO4} = \sum E_{net,i} \times G_{SO4,i}$$

where Y_{SO4} is the total yield of SO_4 molecules (moles m^{-2} sulfide $year^{-1}$) and G_{SO4} is the number of SO_4 molecules produced per m^2 sulfide per Gy radiation. A G_{SO4} value from Lefticariu et al., (2010) is used that is also used in Li et al., (2016) and Altair et al., (2018), which is 2.1×10^{-9} mol m^{-2} Gy^{-1}. However, while the experiments of Lefticariu et al., (2010) were performed under high-energy radiation, they showed that G_{SO4} increases under low-radiation-dose conditions, which correspond to typical radiation doses in natural systems (Li et al., 2016). Furthermore, these experiments only investigated the oxidation, structural damage, and chemical weathering of sulfides exposed to γ radiation. As Lefticariu et al., (2010) note, accounting for increased oxidation, structural damage, and chemical weathering of sulfides from α and β radiation—which typically represent >90% of total irradiated energy—would increase the G_{SO4} value, perhaps significantly. This means once again that the calculated sulfate production rates, and thus supportable sulfate-reducing cell densities herein, are likely conservative estimates. The concentration of sulfate in fluid from radiolytic production is expressed as

$$(4)\ C_{SO4} = Y_{SO4} \times C_{sulfide} \times S_{sulfide} / W$$

where C_{SO4} is the production rate of dissolved sulfate (M year^{-1}), $C_{sulfide}$ is the concentration of sulfide in the rock matrix (volume ratio), and $S_{sulfide}$ is the average specific surface area of sulfides in the rock matrix (m^{-2} sulfide/kg). $C_{sulfide}$ values used in this study are listed in Table 2, which encompasses the values found in martian meteorites (Greenwood et al., 2000b; Greenwood et al., 2000a; Rochette et al., 2001; Lorand et al., 2005; Rochette et al., 2005; Chevrier et al., 2011; Lorand et al., 2015; Baumgartner et al., 2017; Jean-Pierre Lorand et al., 2018b; Jean-Pierre Lorand et al., 2018a). $S_{sulfide}$ values ranging from 2.26×10^{1} m^2 kg^{-1} and 1.41×10^{3} m^2 kg^{-1} are used, which correspond to average sulfide grain sizes of 2-125 μm. The $S_{sulfide}$ values for each meteorite class are assigned based on the range of sulfide grain sizes measured in those martian meteorites (Fig. 1f; Tables 1 & 2). Finally, following Altair et al., (2018), minimum and maximum sulfate-reducing metabolic rates of 5.5×10^{-18} – 3.6×10^{-17} moles cell^{-1} year^{-1} are assumed, which correspond to the minimum and maximum sulfate-reducing metabolic rates estimated in deep subsurface fracture fluids of the gold mines from the Witwatersrand Basin (Lin et al., 2006; Chivian et al., 2008).

2.3 Porosity model

The average porosity ranges for the martian meteorite source regions are estimated using density estimates for the different regions of Mars' crust from orbital gravimetry (Goossens et al., 2017) that are validated by rover gravimetry in Gale crater that estimates a porosity range of 40 ± 6% for the top ~300 meters of bedrock (Lewis et al., 2019). Porosity in this context includes both fracture and pore space within rocks. The orbital gravimetry estimates give average densities of ~1600 kg m^{-3} for the southern highlands, 2400 kg m^{-3} for the northern lowlands, and ~2800 kg m^{-3} for the volcanic bulges. It is assumed that the volcanic bulges and northern

206 lowlands are the possible source regions for the SNCs and the southern highlands are the source
207 region for the regolith breccias (Cassata et al., 2018). In the estimation, an average solid crust
208 matrix density range of 2000-3200 kg m^{-3} is used for the southern highlands crust, consistent
209 with its mineralogy (Ehlmann and Edwards, 2014), and 2600-3200 kg m^{-3} is used for the
210 northern lowlands and volcanic bulges, consistent with volcano-specific orbital gravimetry
211 (Broquet and Wieczorek, 2019). It is assumed the difference between the gravimetry density
212 measurements and rock matrix density estimates is caused by pore space filled with ice or water.
213 The densities add linearly such that $\rho_{bulk} = \rho_{rock}(1-\theta) + \rho_{H2O}(\theta)$ where θ is porosity. This
214 means the composition of the southern highlands rock is assumed to vary, on average, between
215 pure phyllosilicate (~2000 kg m^{-3}) and dense basalt (~3200 kg m^{-3}), while the composition of the
216 northern lowlands and volcanic bulges rocks are assumed to vary between 50-50 phyllosilicate-
217 basalt mixture (~2600 kg m^{-3}) and dense basalt (~3200 kg m^{-3}). Given uncertainties in density
218 estimates from orbital gravimetry, to be conservative, estimated porosities were reduced by 10%.
219 This does not model depth dependence of porosity, but rather the average porosity of the source
220 regions for the individual martian meteorites. This gives approximate average porosity ranges of
221 15-35% for the regolith breccias, 5-15% for the SNCs. The SNC porosity assumptions are
222 supported by images of porous float vesicular basalt rocks in Gusev crater imaged by the Spirit
223 rover (McMahon et al., 2013; McSween, 2015).
224
225 *2.4 Sulfide concentrations*
226 Martian meteorites contain sulfides of both magmatic (pyrrhotite) (Lorand et al., 2005;
227 Lorand et al., 2018b) and hydrothermal (pyrite) (Lorand et al., 2015; Wittmann et al., 2015;
228 Lorand et al., 2018) origins (Sections 2.4 & 2.5). Sulfide abundances range from <0.01-1.0 wt.

%. The assumed sulfide concentration ranges are derived based on these sulfide concentrations found in martian meteorites (Greenwood et al., 2000b; Greenwood et al., 2000a; Rochette et al., 2001; Lorand et al., 2005; Rochette et al., 2005; Chevrier et al., 2011; Franz et al., 2014; Lorand et al., 2015; Hewins et al., 2017; Wang and Becker, 2017; Baumgartner et al., 2017; Jean-Pierre Lorand et al., 2018b; Lorand et al., 2018a; Franz et al., 2019; Hewins et al., 2020) (Fig. 1f; Table 1). Martian meteorites contain variable abundances of sulfides with relatively consistent grain sizes for grains >10 μm. Published abundances for sulfides in martian meteorites, and reported average grain sizes and grain size range, are presented in Table 1. Magmatic sulfides (pyrrhotite) and hydrothermal sulfides (pyrite) are typically associated with SNCs and regolith breccias, respectively (Greenwood et al., 2000b; Greenwood et al., 2000a; Rochette et al., 2001; Lorand et al., 2005; Rochette et al., 2005; Chevrier et al., 2011; Lorand et al., 2015; Baumgartner et al., 2017; Lorand et al., 2018b; Lorand et al., 2018a). Pyrite is much less abundant than pyrrhotite as it was described only in an orthopyroxenite (ALH84001), two chassignites and a few nakhlites (as minor pyrrhotite replacement product), as well as in regolith breccias (as primary hydrothermal precipitate). Sulfide abundances are typically higher in regolith breccias than in SNCs. The listed sulfide abundances are also minimum abundances, as desert weathering of martian meteorite samples causes oxidation of sulfides and partial S losses (Greenwood et al., 2000b; Greenwood et al., 2000a; Rochette et al., 2001; Lorand et al., 2005; Rochette et al., 2005; Chevrier et al., 2011; Lorand et al., 2015; Baumgartner et al., 2017; Lorand et al., 2018b; Lorand et al., 2018a).

The original report of sulfides in Gale crater via CheMin XRD data is no longer supported after recalibration of the data (Morrison et al., 2018), but evolved gas analysis-mass spectroscopy (EGA-MS) (Wong et al., 2020) and sulfur isotope measurements using the Sample Analysis at

Mars (SAM) instrument (Franz et al., 2017) support the presence of sulfides in multiple Gale crater samples. Sulfides in Gale crater are diagenetic/epigenetic, likely resulting from thermal reduction of preexisting sulfates (Franz et al., 2017).

2.5 Sulfide grain sizes

Average grain sizes for sulfides in martian meteorites range from 5-100 μm with occasional outliers up to 400 μm (Fig. 1f; Table 1 and refs. therein). Sulfide grain sizes are relatively consistent across martian meteorite samples (Fig. 1f). A compilation of published measured sulfide average grain sizes and grain size ranges in martian meteorites is presented in Table 1 and plotted in Fig. 1f. It is noteworthy that many of these studies do not consider sulfides <10 μm in diameter, thus these results may skew average sulfide grain sizes towards larger-than-true values. Since sulfate production in the calculations increases as sulfide grain size decreases, as a result of greater specific surface area, this ensures the calculations are conservative. Sulfide grain sizes depend on a wide array of parameters, including temperature, supersaturation of fluids, nucleation rates, and fracturing. For each individual martian meteorite class, the range of measured average sulfide grain sizes in those meteorites are used as the basis for the calculations.

275

276

277

278

279

280

281

282

283

Sample	*Sulfide abundance (wt. %)*	*Average grain size (µm)*	*Grain size min (µm)*	*Grain size max (µm)*	*Publications*	*Type*
NWA 998	0.13	-	20	120	a	Nakhlite
Nakhla	0.07 (0.08)	-	10	50	a,b	Nakhlite
Governardor Valadares	0.06	-	2	25	a	Nakhlite
NWA 817	0.03	-	2	30±15	a	Nakhlite
MIL 03346 And paired samples	0.05	-	-	-	c	Nakhlite
Y000593	0.08	-	-	-	b	Nakhlite
ALH A77005	0.3[d], 0.12[c], 0.19[b]	100	-	-	b-d	Lherzolitic shergottites
LEW 88516	0.3	17.5	-	-	d	Lherzolitic shergottites
Y-293605	0.05	-	-	-	d	Lherzolitic shergottites
Tissint	0.6[e], 0.35[c]	-	<1	200	c,e	Olivine-phyric shergottite
EET A79001-A	0.52[b], 0.28[c]	-	-	-	c	Olivine-phyric shergottite
DaG 476/489	0.45	50	10	100	d	Olivine-phyric shergottites
SaU 005/094	0.30[d], 0.16[c], 0.38[b]	30	10	50	b-d	Olivine-phyric shergottites
Dhofar 019	0.5[d], 0.20[c]	25	-	-	c, d	Olivine-phyric shergottites
NWA 1068/1110	0.8	-	-	-	c, d	Olivine-phyric shergottites
Y-980459	0.1[c], 0.4[b]	30	5	50	b-d, f	Olivine-phyric shergottites
Zagami	0.7[d], 0.24[c], 0.35[b]	<10	100	200	b-d	Basaltic shergottite
Shergotty	0.4	-	100	200	d	Basaltic shergottite
EET A79001-B	0.12	-	-	-	c	Basaltic shergottite
QUE 94201	0.3[d], 0.13[c]	-	-	-	d	Basaltic shergottite
NWA 480	0.24	-	100	200	d	Basaltic shergottite
NWA 856	0.1	-	-	-	d	Basaltic shergottite
Los Angeles	0.67[d], 0.32[c]	-	200	400	d	Basaltic shergottite
Y000097	0.12	-	-	-	b	Lherzolitic shergottite
LAR 12011	0.35	-	-	-	b	Lherzolitic shergottite
LAR12095	0.5	-	-	-	b	Lherzolitic shergottite
Mean of 37	0.21±0.18	-	-	-	c, g	Shergottites

shergottites						
NWA 7533	1±0.1	35	-	-	h, i	Regolith breccia
Chassigny	0.02	20	1-5	30	j	Chassignite
NWA 2737	0.015 ± 0.005	-	3	60	k	Chassignite
NWA 8693	<0.01	-	1	20	l	Chassignite

Table 1 | Sulfide concentrations and grain sizes in martian meteorites. Assume density of 5000 kg/m^3 for sulfide and 3000 kg/m^3 for host rock to convert from vol % to wt %. Franz et al. (2014, 2019) and Wang and Becker (2017) data are calculated from whole-rock S contents assuming 38 wt.% S for pyrrhotite and 54 wt. % for pyrite. Other sulfide abundances are from image analyses on polished thick sections. [a](Chevrier et al., 2011), [b](Wang and Becker, 2017), [c](Franz et al., 2014), [d](Lorand et al., 2005 and refs. therein), [e](Gattacceca et al., 2013), [f](Baumgartner et al., 2017), [g](Franz et al., 2019), [h](Lorand et al., 2015), [i](Lorand et al., 2018a), [j](Lorand et al., 2018b), [k](Lorand et al., 2012), [l](Hewins et al., 2020).

2.6 Radionuclide concentrations

Martian meteorites and remote measurements by the Gamma Ray Spectrometer (GRS) onboard Mars Odyssey (Boynton et al., 2007), which is sensitive to the top ~tens of cm of the martian crust, provide first-order constraints for radionuclide concentrations in the martian subsurface (Fig. 1). Radionuclide concentrations in the top ~tens of cm in the martian crust vary with latitude and longitude (Fig. 1a-b), and volcanic shergottite-nakhlite-chassignite (SNC) martian meteorites generally have lower radionuclide contents than regolith breccias (Fig. 1e) that are likely representative of the Noachian crust (Cassata et al., 2018) (Fig. 1). Elemental concentrations in martian meteorites range from ~0.01-0.4 wt. % K, ~0.01-2 ppm Th, and ~0.003-0.36 ppm U (Onstott et al., 2006; Meyer, 2016) (Fig. 1e). Some U enrichment in these samples is possible through desert contamination (Tarnas et al., 2018). K and Th concentrations estimated from GRS measurements range from ~0.07-0.6 wt. % and ~0.015-1.1 ppm (Boynton et al., 2007; Tarnas et al., 2018), respectively (Fig. 1a-b,e).

For calculations of SO_4 and H_2 production in martian meteorites, the measured values for K, Th, and U in each individual meteorite class were used (Onstott et al., 2006; Meyer, 2016), integrating both the maximum and minimum radionuclide concentration values measured (Fig. 1e; Table 2). The K and Th concentration ranges for SNCs are substantially lower than K and Th concentrations measured in GRS data (Fig. 1e), meaning the majority of the martian crust at depths shallower than ~0.5 m typically has higher radionuclide concentrations than are represented by the SNCs. Following Hahn et al., (2011) and Tarnas et al., (2018), the GRS data are normalized to correct for contributions from Cl, H, and S. K concentrations measured by Mars rovers range from 0.05 wt. % measured by Spirit to 4.4 wt. % measured by Curiosity (Gellert et al., 2004; Deit et al., 2016).

Category	*K_2O concentration (wt %)*	*Th concentration (ppm)*	*U concentration (ppm)*	*Sulfide concentration (vol %)*	*Sulfide grain size (um)*	*Porosity (%)*
Regolith breccia	0.42-0.51[a,b,c]	1.1-2 [a,b,c]	0.29-0.36[a,b,c]	0.6±0.1[a,b,c]	2-100[a,b,c]	15-35
Chassignite	0.036-0.05[d]	0.057-0.13[d]	0.018-0.056[d]	0.006-0.012[e,f]	2-60[e,f]	5-15
Nakhlite	0.11-0.27[d]	0.15-0.42[d]	0.052-0.23[d]	0.018-0.078[g]	2-50[g]	5-15
Shergottite	0.0156-0.35[d]	0.0117-0.57[d]	0.00303-0.12[d]	0.03-0.6[h]	10-200[h]	5-15

Table 2 | Range of values for martian meteorites calculations. [a]Agee et al. (2013), [b]Wittman et al. (2015), [c]Lorand et al. (2018a),[d]Meyer et al. (2016), [e]Lorand et al. (2018b), [f]Lorand et al. (2012), [g]Chevrier et al. (2011), [h]Lorand et al. (2005), [i]Le Deit et al. (2016), [j]Boynton et al. (2007), [k]Hahn et al. (2011), [l]Tarnas et al. (2018), [m]Vaniman et al. (2014). Sulfide grain size excludes the few unusually large sulfide grains reported in each meteorite class.

3.0 Results

3.1 Habitable redox conditions in martian meteorite source regions

The results presented here show that the shergottite, nakhlite, chassignite, and regolith breccia martian meteorite source localities would all produce sufficient redox energy to support sulfate-reducing life where liquid groundwater exists within these lithologies. In all cases, based on the calculations herein, sulfate is the limiting redox nutrient in comparison with H_2. The regolith breccia source locality could support significantly more sulfate-reducing life than the SNC localities because it has higher concentrations of both radionuclides and sulfides. Of the SNCs, the shergottite and nakhlite source localities could support the highest densities of sulfate-reducing cells. Key findings are illustrated in Fig. 2, displayed in Table 3, and are summarized below as:

(1) *Regolith breccia source locality:* The sulfate production rates for the regolith breccia source locality vary from ~$[2 \times 10^{-14}]$ – $[7 \times 10^{-12}]$ moles (kg rock)$^{-1}$ year^{-1}, while H_2 production rates range from ~$[1\text{-}3] \times 10^{-11}$ moles (kg rock)$^{-1}$ year^{-1}, which could support $[7 \times 10^{2}]$-$[1 \times 10^{6}]$ sulfate-reducing cells per kg rock. The regolith breccia source locality would generate the most redox energy for sulfate-reducing microorganisms compared to the other martian meteorite source localities.

(2) *Shergottite source locality*: The sulfate production rates for shergottite source localities vary from ~$[8 \times 10^{-18}]$ – $[2 \times 10^{-13}]$ moles (kg rock)$^{-1}$ year^{-1}, while H_2 production rates range from ~$[4 \times 10^{-14}]$-$[4 \times 10^{-12}]$ moles (kg rock)$^{-1}$ year^{-1}, which could support $[2 \times 10^{-1}]$-$[3 \times 10^{4}]$ sulfate-reducing cells per kg rock wherever liquid water exists.

(3) *Nakhlite source locality:* The sulfate production rates for nakhlite source localities vary from ~$[1 \times 10^{-16}]$ – $[2 \times 10^{-13}]$ moles (kg rock)$^{-1}$ year^{-1}, while H_2 production rates range

from ~[5×10^{-13}]-[6×10^{-12}] moles (kg rock)$^{-1}$ year^{-1}, which could support [3]-[3×10^{4}] sulfate-reducing cells per kg rock.

(4) *Chassignite source locality:* The sulfate production rates for chassignite source localities vary from ~[1×10^{-17}]– [6×10^{-15}] moles (kg rock)$^{-1}$ year^{-1}, while H_2 production rates range from ~[2×10^{-13}]-[2×10^{-12}] moles (kg rock)$^{-1}$ year^{-1}, which could support [4×10^{-1}]-[1×10^{3}] sulfate-reducing cells per kg rock.

	Radiolytic H_2 production rate in moles (kg rock)$^{-1}$ year^{-1}	*Radiolytic Sulfate production rate in moles (kg rock)$^{-1}$ year^{-1}*	*Supportable sulfate-reducing cell density in cells (kg rock)$^{-1}$*
Regolith breccia	~[1-3] × 10^{-11}	~[2×10^{-14}] – [7×10^{-12}]	[7×10^{2}]-[1×10^{6}]
Shergottite	~[4×10^{-14}]-[4×10^{-12}]	~[8×10^{-18}] – [2×10^{-13}]	[2×10^{-1}]-[3×10^{4}]
Nakhlite	~[5×10^{-13}]-[6×10^{-12}]	~[1×10^{-16}] – [2×10^{-13}]	[3]-[3×10^{4}]
Chassignite	~[2×10^{-13}]-[2×10^{-12}]	~[1×10^{-17}]– [6×10^{-15}]	[4×10^{-1}]-[1×10^{3}]

Table 3 | Estimated H_2 and sulfate production rates for martian meteorite source regions and associated supportable sulfate-reducing cell densities.

The sulfate production rates from these calculations are several orders of magnitude lower than those of Lefticariu et al., (2010) because those authors assumed 5-10 wt. % pyrite in the martian crust, while this study uses lower sulfide concentrations based on measured values from martian meteorites (Fig. 1f, Table 1). Because the model uses the lowest and highest measured sulfate-reducing metabolic rates in Witwatersrand Basin for calculating cell density estimates (Lin et al., 2006; Chivian et al., 2008), there is a difference between the estimated maximum and minimum range for sulfate production rates and the estimated maximum and minimum range for number of supportable sulfate-reducing cells per kg rock. H_2 production estimates, in units of H_2

dissolved in water, range from 0.002-0.165 nM H_2/year. This compares to estimates by Dzaugis et al., (2018) of 0.001-1.2 nM H_2/year for proposed Mars landing sites. The differences in the dissolved H_2 estimates between this study and Dzaugis et al., (2018) derive from differences in radionuclide concentrations and porosity used for calculations in the two studies.

The number of supportable sulfate-reducing cells per kg rock in the nakhlite, shergottite, and regolith breccia source localities are comparable to those found in Earth's deep subsurface ($\sim 10^4 - 10^6$ cells per kg rock; Onstott et al., 2019) (Fig. 2). Estimates for the chassignite source locality meanwhile are slightly lower ($\sim 10^1 - 10^3$ cells per kg rock). In all cases, sulfate is the redox nutrient that limits sustainable cell densities, and as such estimated cell densities are most sensitive to estimated sulfate production rates. The martian regolith breccia NWA 7034 and one of its paired samples, NWA 7533, contain the highest radionuclide and sulfide concentrations of the currently known martian meteorites, and thus their source locality would host sulfate production rates capable of supporting the greatest density of sulfate-reducing microorganisms relative to other known martian meteorites. Regolith breccia meteorites are likely representative of the southern highlands, which is a major fraction of Mars' total crustal volume. The results presented here support growing evidence that the subsurface is potentially the largest, longest-lived, and most consistently habitable environment on Mars (Michalski et al., 2018; Michalski et al., 2013; Onstott et al., 2019; Tarnas et al., 2018) and could serve as a refugia for any life that ever existed on the martian surface (National Academies of Sciences, Engineering, and Medicine et al., 2018; Michalski et al., 2018). Other viable processes could produce redox nutrients to sustain additional metabolisms in the martian subsurface, including H_2 and CH_4 production via serpentinization and Fischer-Tropsch-type synthesis, respectively (e.g. Warr et al., 2019), atmospheric O_2 dissolution (Stamenković et al., 2018), atmospheric H_2 and CO dissolution

(Weiss et al., 2000), as well as Fe^{2+} and Fe^{3+} from minerals (Onstott et al., 2019). If sulfides are not present in the rock matrix, these other reactions may be favorable over sulfate reduction. These results provide scientific justification for future missions to search for signs of extant life in the martian subsurface—which is an intriguing next frontier for planetary exploration (National Academies of Sciences, Engineering, and Medicine et al., 2018; Stamenković et al., 2019)—and identifies key characteristics of optimal regions for future landing sites.

Even the relatively small sampling of Mars' petrologic diversity via four martian meteorite classes (shergottites, nakhlites, chassignites, regolith breccias) shows a wide range in redox energy production rates from these different rock types/localities (Fig. 2). Some of these localities, such as the source regions for regolith breccias, shergottites, and nakhlites could support comparable concentrations of extant life to those found in Earth's deep subsurface (Onstott et al., 2003; Cockell et al., 2012; Onstott et al., 2019). As is demonstrated by the diversity of radionuclide concentrations, sulfide concentrations, and sulfide grain sizes in martian meteorites, some regions of the martian crust will support higher sulfate-reducing cell densities than others. Because sulfate is likely the limiting nutrient for hydrogenotrophic sulfate-reducing metabolisms in a martian subsurface biosphere rather than H_2, the highest concentrations of sulfate-reducing microorganisms would exist in a water-bearing crustal section with high sulfide abundance, low sulfide grain sizes, and relatively high radionuclide concentrations. Regions rich in zeolites, which enhance radiolytic gas production (Kumagai et al., 2013), would also sustain higher sulfate-reducing bacteria concentrations. Future missions should focus on characterizing where these criteria are met, as these would be prime landing site targets for extant life investigation from a redox energy perspective.

4.0 Discussion

4.1 Potential for higher cell densities elsewhere on Mars

The possibility of relatively high sulfide concentrations on Mars has been recognized for decades due to the presence of ultramafic lithologies there (Burns and Fisher, 1990; Baumgartner et al., 2015; Humayun et al., 2019) (Section 4.2). Concentration of magmatic sulfides are assumed to derive from assimilation of crustal sulfates and/or S-rich regolith in lava flows, as sampled by nakhlites, which likely crystallized from a sulfide-saturated melt after this assimilation (Franz et al., 2014; Mari et al., 2019). Additional evidence for the existence of concentrated martian sulfides has continued to accrue in the form of sulfides in martian meteorites (Table 1 and refs. therein), in Gale crater (Franz et al., 2017; Wong et al., 2020), the prevalence of sulfate-hematite assemblages on the martian surface (e.g. Wiseman et al., 2008), which may or may not have formed as weathering products of sulfides (e.g. Zolotov and Shock, 2005), verifiable orbital detections of serpentine outcrops in Noachian terrains (Leask et al., 2018), which are often associated with formation of reduced sulfides and metal alloys on Earth (e.g. Economou and Naldrett, 1984; Thalhammer et al., 1986; Shiga, 1987; Auclair et al., 1993; Wafik et al., 2001; Marques et al., 2007), Cu concentrations in Gale crater that are likely caused by presence of sulfides (Payré et al., 2019), and the low oxygen fugacity (Mari et al., 2019 and refs. therein) and high sulfur fugacity of the ancient martian mantle relative to Earth's (Wang and Becker, 2017; Mari et al., 2019 and refs. therein). Pyrrhotite hosts magnetization in multiple classes of martian meteorites (Rochette et al., 2005 and refs. therein) and thus at high enough concentrations its subsurface presence could explain Mars' crustal magnetic field anomalies (Langlais et al., 2019; Johnson et al., 2020).

High concentrations of sulfides could form via differentiation of sulfide-saturated lavas that were contaminated by crustal assimilation of sulfates (Burns and Fisher, 1990; Baumgartner et al., 2015) as occurred in nakhlite lava flows (Franz et al., 2014; Mari et al., 2019), differentiation of impact melt accompanied by crustal sulfur assimilation as occurred in Sudbury, Ontario (e.g. Therriault et al., 2002), later hydrothermal sulfide precipitation with or without serpentinization, as is recorded in regolith breccia martian meteorites (Lorand et al., 2015), or differentiated intrusions (Fig. 3; Section 4.3). Once formed, fluid fracture networks within such sulfide-rich regions in the subsurface of Mars could support high concentrations of radiolytically-fueled sulfate-reducing microorganisms and would be key locations to investigate the possibility of extant life on Mars.

4.2 Evidence for concentrated sulfides on Mars

The conclusions from this study do not require concentrated sulfides on Mars, but rather are based on the large body of data for disseminated sulfides on Mars. As such, the estimates are appropriately conservative and are consistent with the body of lithological and geochemical data available. The presence of concentrated sulfide deposits on Mars can be considered, however, and supporting evidence includes (1) sulfur assimilation and sulfide saturation in nakhlite melts (Franz et al., 2014; Mari et al., 2019), (2) geologic evidence for high sulfide concentrations elsewhere in the martian crust based on expected mantle oxygen (Stanley et al., 2011; Armstrong et al., 2015) and sulfur (Ding et al., 2014) fugacities, (3) surface evidence for sulfide oxidation (Zolotov and Shock, 2005; Dehouck et al., 2012; Vaniman et al., 2014), and (4) orbital detections of past serpentinization (Ehlmann et al., 2010; Leask et al., 2018), which produces reducing fluids and is often associated with generation of hydrothermal sulfide deposits on Earth

458 (e.g. Economou and Naldrett, 1984; Thalhammer et al., 1986; Shiga, 1987; Auclair et al., 1993;
459 Wafik et al., 2001; Marques et al., 2007).

460 1. Nakhlites likely crystallized from a sulfide saturated melt after S assimilation from
461 the crust/regolith based on $\Delta^{33}S$, $\delta^{34}S$, and highly siderophile element (HSE) patterns
462 (Mari et al., 2019). Some amount of sulfur assimilation from S-rich regolith occurred
463 after the nakhlite lavas were emplaced on or near the martian surface (Franz et al.,
464 2014; Mari et al., 2019). Nakhlites are the only SNC meteorite class known to likely
465 have crystallized from a sulfide-saturated melt, as shergottites crystallized from
466 sulfide undersaturated parent magmas (Wang and Becker, 2017). Still, 1/3 of volcanic
467 martian meteorite classes exhibiting geochemical characteristics consistent with
468 crystallization from a sulfide saturated melt implies that characteristically similar
469 volcanism could have occurred throughout Mars' history. Sulfates are prevalent
470 across the surface of Mars (Ehlmann and Edwards, 2014), S-rich regolith is
471 effectively ubiquitous across the surface (Clark et al., 1976; Foley et al., 2003), and
472 elemental sulfur concentrations measured by GRS range from 0.7-3.2 wt. % at GRS
473 spatial resolution (McLennan et al., 2010), thus a substantial amount of sulfur for
474 accumulation by lavas commonly exists on the martian surface. Therefore, it is likely
475 that lavas saturated with respect to sulfide after assimilation of S from the
476 crust/regolith—similar to those from which nakhlites crystallized—were common
477 throughout Mars' history, thus resulting in the formation of high sulfide concentration
478 zones.

479 2. The martian mantle is generally expected to be more reducing than Earth's (Stanley et
480 al., 2011; Armstrong et al., 2015), with estimates for mantle oxygen fugacity based on

basalts measured in Gusev crater varying from iron-wüstite (IW) to IW+1 (Stanley et al., 2011). Oxygen fugacity estimates from shergottites are estimated to be [QFM-4]-[QFM-1] (Herd, 2003), and from nakhlites are ~QFM (Mari et al., 2019). Earth's mantle has an oxygen fugacity range of [QFM-1]-[QFM+1] (Blundy et al., 1991; Brounce et al., 2017). Still, on Earth, pyrrhotite is found in volcanic rocks derived from partial melting of a more oxidized mantle relative to Mars (e.g. Desborough et al., 1968; Whitney, 1984), though concentrations are typically higher in silicic magmas than basalt, the latter of which is more common on Mars. Thus, magmatic sulfides are expected in some volcanic rocks derived from the wide variability in melt oxygen fugacities from the martian mantle. Martian mantle sulfur abundance estimates range from ~400-2200 ppm (Wang and Becker, 2017), while Earth's mantle sulfur abundance is ~250 ppm (McDonough and Sun, 1995). Additional sulfur is incorporated into martian melts via crustal assimilation of sulfates and/or S-rich regolith, as occurred in the nakhlite lavas (Franz et al., 2014; Mari et al., 2019). As such, sulfur activity in martian melts is typically higher than in most melts on Earth, while oxygen fugacity is lower than in most melts on Earth, both of which increase the likelihood of sulfide precipitation.

3. Sulfide oxidation has been invoked to explain multiple mineral assemblages found on the martian surface (King and McSween, 2005), including the hematite enrichment in Meridiani Planum (Zolotov and Shock, 2005), the Burns formation –a sulfate-rich sandstone in Merdiani Planum (Zolotov and Shock, 2005), sulfate-carbonate assemblages found using orbital hyperspectral data (Dehouck et al., 2012), akaganeite detections made from orbit (Carter et al., 2015), and acidic fluid diagenetic mineral

assemblages detected by the Curiosity rover (Rampe et al., 2017). In its type locality on Earth, akaganeite forms as an alteration product of pyrrhotite (Nambu, 1968). To concentrate the abundances of sulfur needed to form the Burns formation, pre-concentration of sulfur via magmatic or hydrothermal sulfides may be required (Zolotov and Shock, 2005). Furthermore, oxidation of sulfides to form the acid-mine-drainage-like mineral assemblages of sulfates and oxides seen on the martian surface provides a functional hypothesis for generation of these assemblages. Formation of concentrated sulfides could have occurred on Mars via differentiation/crustal assimilation from ultramafic lavas (Burns and Fisher, 1990), the existence of which is supported by possible observations of ultramafic volcanism on the martian surface (Ruff et al., 2014; Ruff et al., 2019; Kremer et al., 2019), ultramafic lithologies in martian meteorites (Burns and Fisher, 1990), and evidence that nakhlites crystallized from sulfide-saturated melts after S assimilation from the crust/regolith (Franz et al., 2014; Mari et al., 2019).

4. Mg-rich serpentine has been detected on Mars using CRISM hyperspectral images (Ehlmann et al., 2010; Leask et al., 2018), but most of these detections have been called into question after discovery of a 2.1 μm spectral artifact in CRISM TRR3 data that can resemble the diagnostic absorption feature of Mg-rich serpentine (Leask et al., 2018). Still, at least 3 Mg-rich serpentine detections have been validated as unrelated to this artifact (Leask et al., 2018), demonstrating that serpentinization has occurred on Mars. The fluids generated via serpentinization are highly reducing, which can cause precipitation of reduced alloys and minerals such as awaruite (Lorand, 1985; Sleep et al., 2004) (NiFe alloy) and sulfides (Economou and Naldrett,

1984; Thalhammer et al., 1986; Shiga, 1987; Auclair et al., 1993; Wafik et al., 2001; Marques et al., 2007). As such, serpentinization would have generated reducing fluids on Mars that could have precipitated and concentrated sulfide minerals, making regions containing serpentine potential 'hotzones' for both ancient chemolithotrophic life that consumed H_2 from serpentinization, as well as modern chemolithotrophic life that may consume H_2 and SO_4 from radiolysis in sulfide-rich zones.

4.3 Possible settings of concentrated sulfides on Mars

1. *Differentiated impact melt sheets:* The Sudbury Impact Structure in Ontario, Canada is one of the three largest discovered impact structures on Earth—the others being Chicxulub and Vredefort—and hosts concentrations of sulfides of high economic value. Sulfides were concentrated via gravitational differentiation from the impact melt sheet (Zieg and Marsh, 2005). Sulfur was likely introduced to the impact melt via assimilation from the surrounding country rock during the depressurization melting that formed the Sudbury Igneous Complex (Walker et al., 1991; Dickin et al., 1992; Mungall et al., 2004). Because of the prevalence of sulfur on Mars in the form of sulfates and S-rich regolith, and the larger number of preserved impact structures on Mars relative to Earth, Sudbury-type differentiated impact melt sheet sulfide concentrations may be more common on Mars than they are on Earth (West and Clarke, 2010) (Fig. 3 Setting 1).
2. *Layered intrusions*: Sulfides are commonly concentrated in ultramafic-to-mafic layered intrusions on Earth, such as the Bushveld Igneous Complex in South Africa (Gain and Mostert, 1982), Voisey's Bay in Canada (Evans-Lamswood et al., 2000),

Jinchuan in China (Chai and Naldrett, 1992), and the Noril'sk-Talnakh deposits in Siberia (Arndt et al., 2003). Sulfides are typically concentrated as residue in restricted conduits/channels, and thus are often concentrated at the base of the layered intrusion, in sills, or in stratiform reef-style deposits (Lightfoot and Evans-Lamswood, 2015). Such intrusions typically form in intracratonic settings, often via mantle plume activity (Barnes et al., 2017). This is similar to settings of non-subvolcanic and subvolcanic intrusions formed on Mars, which is a single-plate planet. There is evidence for ultramafic volcanism on Mars (Ruff et al., 2019; Kremer et al., 2019) and basaltic volcanism is prevalent across the entire planet (Bandfield et al., 2000). Mantle plumes have caused volcanism on Mars, likely forming the Tharsis and Elysium volcanic bulges (Fuller and Head, 2003; Redmond and King, 2004; Hynek et al., 2011). It is thus plausible that both subvolcanic and non-subvolcanic ultramafic-to-mafic magmatic intrusions exist on Mars, providing structures for potential concentration of sulfides (Fig. 3 Settings 2 & 7).

3. *Hydrothermal sulfides*. Sulfides are concentrated by hydrothermal fluids that are S-rich and reducing. Many hydrothermally-formed sulfide deposits are associated with serpentinites, due to the highly reducing fluids formed during the process of serpentinization (Lorand, 1985; Sleep et al., 2004) causing formation of metal alloys (Lorand, 1985) and sulfides (Economou and Naldrett, 1984; Thalhammer et al., 1986; Shiga, 1987; Auclair et al., 1993; Wafik et al., 2001; Marques et al., 2007). Hydrothermal sulfides are found in regolith breccia martian meteorites (Lorand et al., 2015; Wittmann et al., 2015; Hewins et al., 2017; Jean-Pierre Lorand et al., 2018a). Minerals potentially produced by hydrothermal alteration, including smectites,

carbonates, chlorite, hydrated silica, and zeolites (Ehlmann et al., 2009), and small amounts of Mg-serpentine (Ehlmann et al., 2010; Leask et al., 2018) are detected on the martian surface from orbit using CRISM. Evidence for past hydrothermal alteration has been seen by every Mars rover. NASA's Opportunity rover observed evidence for multiple diagenetic episodes in the Burns Formation (McLennan et al., 2005), as well as hydrothermal alteration of bedrock due to meteorite impact at Endeavour crater (Squyres et al., 2012; Arvidson et al., 2014). NASA's Spirit rover observed carbonate-bearing olivine-rich rocks (Comanche) formed via alteration of ultramafic tuff (Algonquin) (Morris et al., 2010; Ruff et al., 2014), silica deposits (Ruff et al., 2011) that likely formed in hot spring settings (Ruff and Farmer, 2016; Ruff et al., 2019), and hydrothermal alteration of Home Plate resulting in precipitation of silica (Squyres et al., 2008). NASA's Curiosity rover has found evidence for multiple diagenetic episodes in the stratigraphy of Mount Sharp, including cross-cutting Ca-sulfate veins (Yen et al., 2017), jarosite veins dated to 2.1 ± 4 Gyr (Martin et al., 2017), and evidence for diagenetic episodes that cross-cut multiple stratigraphically distinct units (Sheppard et al., 2019). Sulfides could also be concentrated via hydrothermal activity during submarine volcanism –as likely occurred in Eridania Basin (Michalski et al., 2017). As such, hydrothermal alteration has occurred on Mars in a wide variety of geochemical settings, including some that precipitated pyrite in regolith breccias (Lorand et al., 2015; Wittmann et al., 2015; Hewins et al., 2017; Jean-Pierre Lorand et al., 2018a), and some that formed serpentinite (Ehlmann et al., 2010; Leask et al., 2018). It is plausible that higher concentrations of sulfides than those found in NWA 7533 and NWA 7034— which

were ejected from Mars by the same impact event (Wittmann et al., 2015)—could form from hydrothermal alteration in other regions of the martian crust (Fig. 3 Settings 3 & 5).

4. *Sulfide-bearing sediments.* Mount Sharp in Gale crater is an example of a sulfide-bearing sediment mound on Mars (McAdam et al., 2014; Franz et al., 2017; Wong et al., 2020) (Fig. 3 Setting 4). These sulfides are diagenetic/epigenetic, likely resulting from thermal reduction of preexisting sulfates (Franz et al., 2017). It is possible that a similar sulfate thermal reduction process could occur in other sulfate-bearing martian sediments, which are widespread (Ehlmann and Edwards, 2014), thus generating a higher concentration of sulfides in those localities. Cu-enrichments in Gale crater are potentially due to presence of detrital sulfides (Payré et al., 2019). It is therefore plausible that sulfides could be concentrated in martian sediments in detrital form and also via diagenetic processes.

5. *Differentiated ultramafic-to-mafic lava flows.* Examples of sulfide concentrations in komatiitic lava flows on Earth include the Kambalda and Perseverance deposits in Australia. Sulfides are also concentrated picrites, including the Pechenga deposits in Russia (Barnes et al., 2017). Due to the presence of ultramafic lithologies in martian meteorites, the possibility of sulfide concentration in komatiite-type settings has been known for decades (Burns and Fisher, 1990). Since then, further evidence for ultramafic volcanism on Mars has been presented (Ruff et al., 2014; Ruff et al., 2019; Kremer et al., 2019). The magmas that precipitated the nakhlites assimilated sulfur from the crust, forming a sulfide-saturated melt (Franz et al., 2014; Mari et al., 2019). Thus, there is already evidence for some degree of sulfide concentration in

differentiated ultramafic-to-mafic lava flows on Mars via the martian meteorites (Fig. 3 Setting 6).

5.0 Conclusions

The results presented here demonstrate that radiolysis in the martian meteorite source lithologies would produce sufficient H_2 and sulfate to sustain sulfate-reducing bacteria wherever groundwater is present. The regolith breccia source lithology, which is within the southern highlands (Cassata et al., 2018), could sustain the highest concentrations of sulfate-reducing bacteria, with shergottite and nakhlite lithologies supporting the second highest concentrations. The calculated supportable sulfate-reducing bacteria densities in the regolith breccia, shergottite, and nakhlite source lithologies are comparable to those measured in Earth's deep subsurface (Table 3; Fig. 2).

If Earth-like chemolithotrophic life ever existed on Mars and survived until present, it could potentially be sustained in these subsurface regions by harnessing the same radiolytically-derived energy that drives the metabolisms of microbial ecosystems on Earth sustained in groundwaters $>10^6$-10^9 years old (Lin et al., 2006; Chivian et al., 2008; Lollar et al., 2019). Furthermore, this subsurface environment has likely remained habitable since the Noachian (Tarnas et al., 2018), making it the longest-lived habitable environment on Mars and the most likely refugia for any life on the planet (National Academies of Sciences, Engineering, and Medicine et al., 2018; Michalski et al., 2018). The parameters outlined here –radionuclide abundance, sulfide abundance, average sulfide grain size, and porosity—along with characterization of the locations of liquid groundwater, can be used to constrain an optimal landing site for a mission to detect Earth-like extant sulfate-reducing martian life in the subsurface. Additional microbial

metabolisms, for which redox energy availability is more difficult to model, could also exist in the martian subsurface, as they do in Earth's subsurface, potentially increasing the measured biomass in any subsurface region that contains groundwater. This should be considered in the context of future extant life detection missions to Mars.

Figures

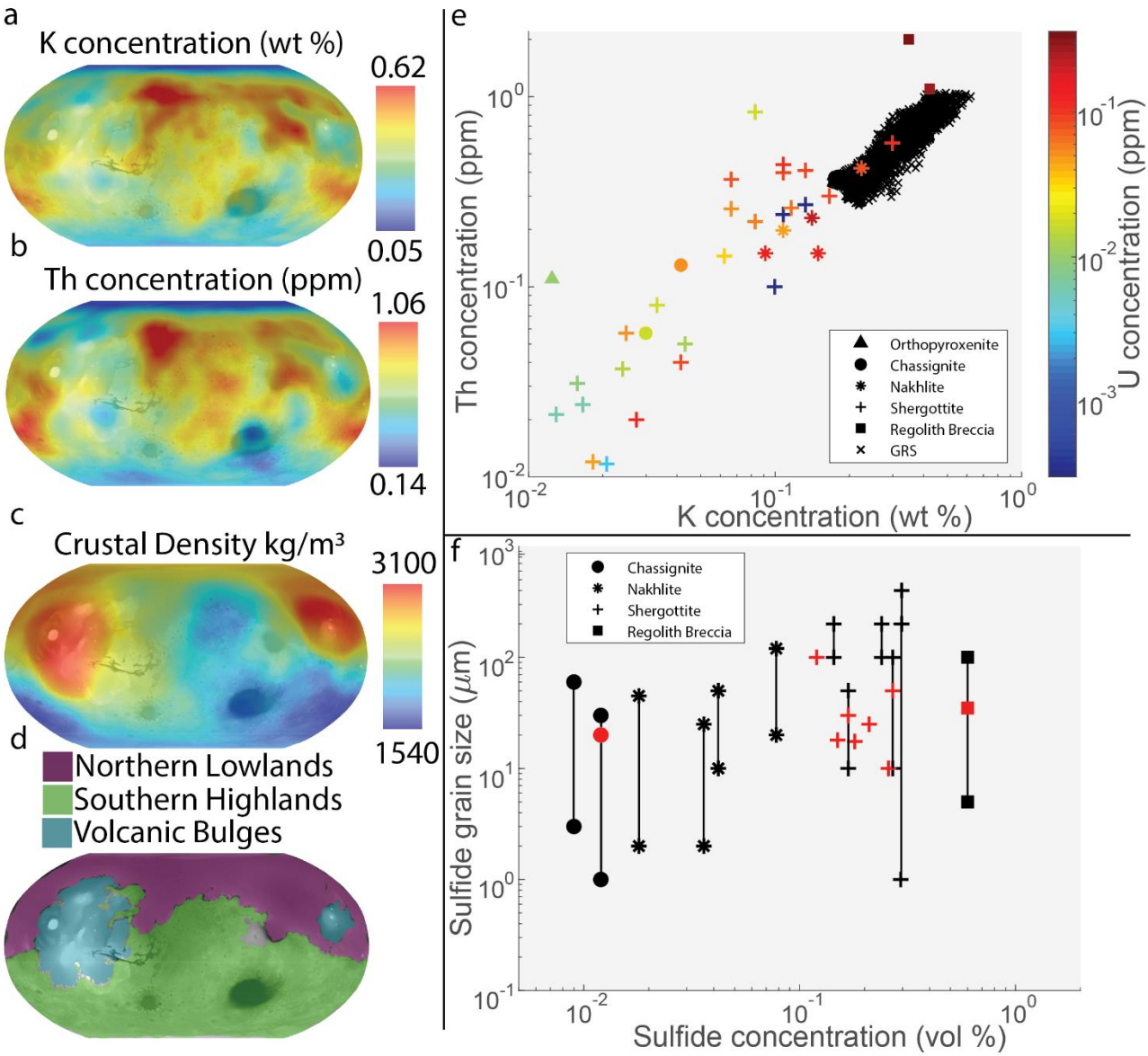

Figure 1 | Model input data. (a) K concentration (wt. %) from GRS data, corrected for contributions Cl, H, and S (Boynton et al., 2007; Tarnas et al., 2018). (b) Th concentration (ppm) from GRS data, corrected for contributions Cl, H, and S (Boynton et al., 2007; Tarnas et al., 2018). (c) Possible crustal density estimates from orbital gravimetry (Goossens et al., 2017) that are supported by rover gravimetry (Lewis et al., 2019). (d) Division of Mars into 3 different regions. (e) Radionuclide abundances in martian meteorites (Meyer, 2016) and GRS data from 60ºS-60ºN, where near surface ice does not contaminate measurements (Boynton et al., 2007; Tarnas et al., 2018). The lower spatial resolution of GRS data (100s of km) means the calculated K and Th concentrations are more closely clustered than in the martian meteorites. There are also no U concentration measurements from GRS data, thus the color is black. (f) Sulfide concentrations and grain sizes in martian meteorites are compiled and referenced in Table 1. Black symbols show the maximum and minimum reported grain sizes, while red symbols show the reported average grain size.

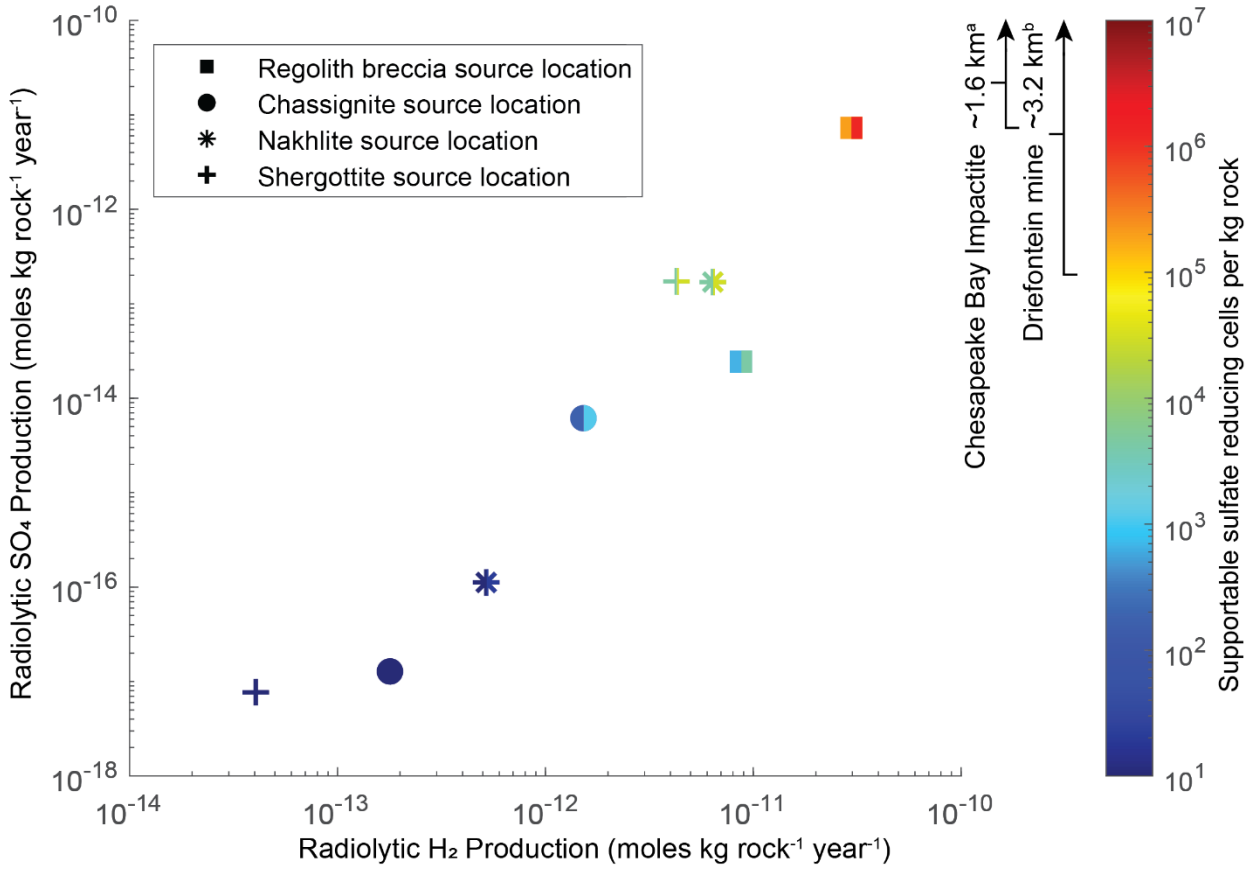

663

664 **Figure 2 | Radiolytic redox energy production and number of supportable sulfate-reducing**
665 **cells in Mars meteorite source regions.** The datapoints represent the highest and lowest
666 endmembers for each given category, with the assumed values for the calculations presented in
667 Table 2. The different colors of the same datapoints represent the supportable sulfate-reducing
668 cells per kg rock assuming the highest and lowest metabolic rates observed in Earth's deep
669 subsurface ($5.5 \times 10^{-18} - 3.6 \times 10^{-17}$ moles cell^{-1} year^{-1}) (Lin et al., 2006; Chivian et al., 2008).
670 Cell density measurements from Earth's deep subsurface come from [a](Cockell et al., 2012),
671 [b](Onstott et al., 2003).

672

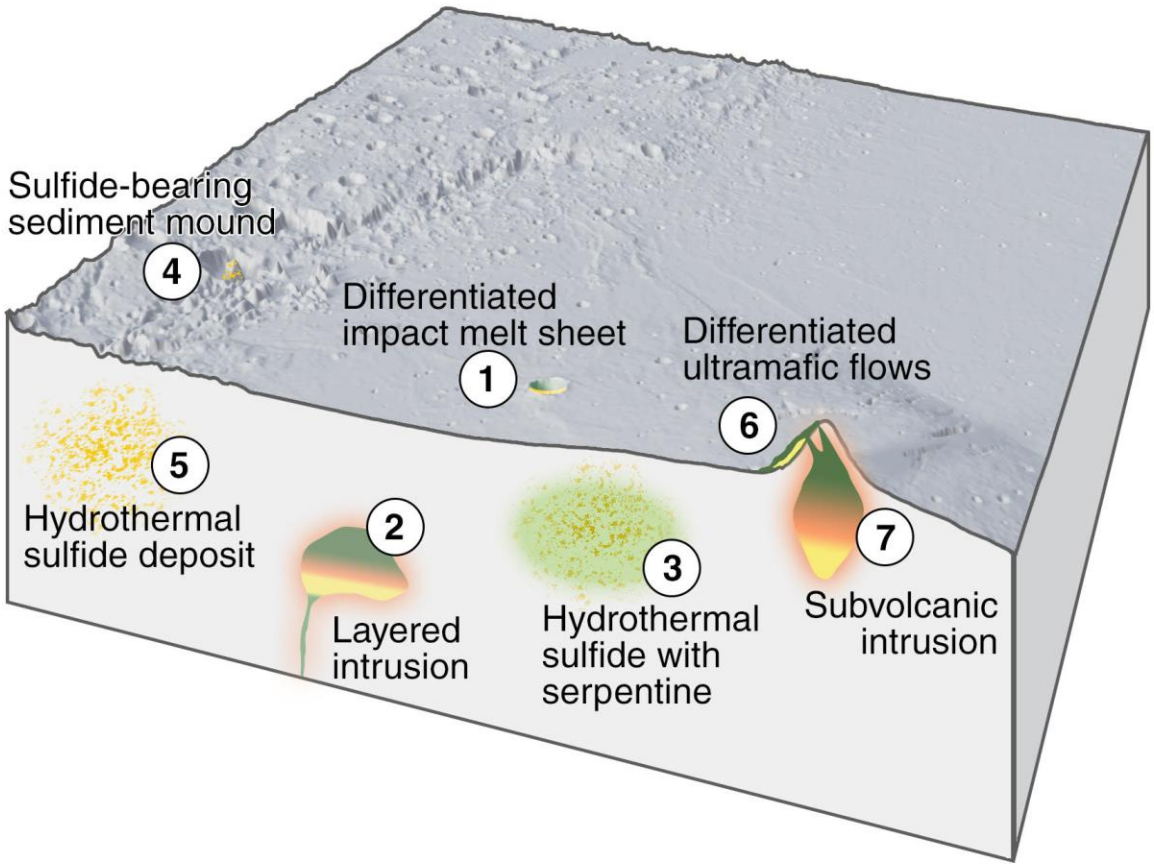

673

674 **Figure 3 | Possible sulfide concentration settings on Mars in addition to those found in**
675 **martian meteorites.** Topographic cross-section of Mars using data from the Mars Orbital Laser
676 Altimeter (MOLA) from 10ºS, 141ºE; 29ºN, 149ºE; 4ºS, 104ºE; 35ºN, 96ºE. See Materials and
677 Methods for discussion of possible sulfide concentration settings on Mars, in addition to sulfide
678 concentrations found in martian meteorites that are used for calculations in this study. (1)
679 Differentiated impact melt sheet similar to sulfide concentrations at the Sudbury Impact
680 Structure in Canada (Therriault et al., 2002). (2) Sulfide concentration in layered intrusion,
681 similar to Bushveld Igneous Complex in South Africa and many other localities on Earth. (3)
682 Sulfide hydrothermally concentrated in serpentinite, similar to many ophiolite localities on Earth.
683 Mg-serpentine has been detected on Mars (Leask et al., 2018). (4) Sulfide concentrations in

sediments, such as those in Gale crater (Franz et al., 2017; Wong et al., 2020). (5) Sulfide hydrothermally concentrated without associated serpentinite minerals, such as those in regolith breccia martian meteorites (Lorand et al., 2005; Lorand et al., 2015; Jean-Pierre Lorand et al., 2018b; Jean-Pierre Lorand et al., 2018a). (6) Concentrations of sulfides in differentiated ultramafic-to-mafic lava flows, as occurs in many localities on Earth including the Kambalda and Perseverance deposits in Australia. Sulfides are also concentrated in picrites, including the Pechenga deposits in Russia. This is a possible formation setting for nakhlites, which crystallized from sulfide saturated magmas after assimilation of S from the crust/regolith (Franz et al., 2014; Mari et al., 2019). (7) Concentration of sulfides in ultramafic-to-mafic subvolcanic intrusions beneath volcanic provinces such as Tharsis, Elysium, and Syrtis Major.

Acknowledgements

We thank Norman Sleep and an anonymous reviewer for feedback that improved the quality of this manuscript. We thank Paul Niles, Ralph Milliken, and Steven D'Hondt for discussions. Thanks to the Astromaterial Curation Group at NASA JSC, especially Kevin Righter, for providing a compilation table of martian meteorite elemental abundances. We thank Paul Niles, Ralph Milliken, and Steven D'Hondt for discussions. J.D.T. gratefully acknowledges support from the NASA Postdoctoral Program and a Brown University Dissertation Fellowship. J.F.M., B.S.L., V.S., and J.R.M. acknowledge support from the Canadian Institute for Advanced Research (CIFAR).

References

Adamiec G. and Aitken M. (1998) Dose-rate conversion factors: Update: Ancient TL, v. 16. *ArcheoSciences, revue d'archéométrie* **32**, 51–58.

708 Altair T., de Avellar M. G. B., Rodrigues F. and Galante D. (2018) Microbial habitability of Europa
709 sustained by radioactive sources. *Scientific Reports* **8**, 1–8.

710 Armstrong L. S., Hirschmann M. M., Stanley B. D., Falksen E. G. and Jacobsen S. D. (2015)
711 Speciation and solubility of reduced C–O–H–N volatiles in mafic melt: Implications for
712 volcanism, atmospheric evolution, and deep volatile cycles in the terrestrial planets.
713 *Geochimica et Cosmochimica Acta* **171**, 283–302.

714 Arndt N. T., Czamanske G. K., Walker R. J., Chauvel C. and Fedorenko V. A. (2003) Geochemistry
715 and Origin of the Intrusive Hosts of the Noril'sk-Talnakh Cu-Ni-PGE Sulfide Deposits.
716 *Economic Geology* **98**, 495–515.

717 Arvidson R. E., Squyres S. W., Bell J. F., Catalano J. G., Clark B. C., Crumpler L. S., Souza P. A. de,
718 Fairén A. G., Farrand W. H., Fox V. K., Gellert R., Ghosh A., Golombek M. P., Grotzinger J.
719 P., Guinness E. A., Herkenhoff K. E., Jolliff B. L., Knoll A. H., Li R., McLennan S. M., Ming
720 D. W., Mittlefehldt D. W., Moore J. M., Morris R. V., Murchie S. L., Parker T. J., Paulsen
721 G., Rice J. W., Ruff S. W., Smith M. D. and Wolff M. J. (2014) Ancient Aqueous
722 Environments at Endeavour Crater, Mars. *Science* **343**. Available at:
723 https://science.sciencemag.org/content/343/6169/1248097 [Accessed July 9, 2020].

724 Auclair M., Gauthier M., Trottier J., Jebrak M. and Chartrand F. (1993) Mineralogy,
725 geochemistry, and paragenesis of the Eastern Metals serpentinite-associated Ni-Cu-Zn
726 deposit, Quebec Appalachians. *Economic Geology* **88**, 123–138.

727 Bandfield J. L., Hamilton V. E. and Christensen P. R. (2000) A Global View of Martian Surface
728 Compositions from MGS-TES. *Science* **287**, 1626–1630.

729 Barnes S. J., Holwell D. A. and Vaillant M. L. (2017) Magmatic Sulfide Ore Deposits. *Elements* **13**,
730 89–95.

731 Baumgartner R. J., Fiorentini M. L., Baratoux D., Micklethwaite S., Sener A. K., Lorand J. P. and
732 McCuaig T. C. (2015) Magmatic controls on the genesis of Ni–Cu±(PGE) sulphide
733 mineralisation on Mars. *Ore Geology Reviews* **65**, 400–412.

734 Baumgartner R. J., Fiorentini M. L., Lorand J.-P., Baratoux D., Zaccarini F., Ferrière L., Prašek M.
735 K. and Sener K. (2017) The role of sulfides in the fractionation of highly siderophile and
736 chalcophile elements during the formation of martian shergottite meteorites.
737 *Geochimica et Cosmochimica Acta* **210**, 1–24.

738 Blundy J. D., Brodholt J. P. and Wood B. J. (1991) Carbon–fluid equilibria and the oxidation state
739 of the upper mantle. *Nature* **349**, 321–324.

740 Boynton W. V., Taylor G. J., Evans L. G., Reedy R. C., Starr R., Janes D. M., Kerry K. E., Drake D.
741 M., Kim K. J., Williams R. M. S., Crombie M. K., Dohm J. M., Baker V., Metzger A. E.,
742 Karunatillake S., Keller J. M., Newsom H. E., Arnold J. R., Brückner J., Englert P. a. J.,
743 Gasnault O., Sprague A. L., Mitrofanov I., Squyres S. W., Trombka J. I., d'Uston L., Wänke

744 H. and Hamara D. K. (2007) Concentration of H, Si, Cl, K, Fe, and Th in the low- and mid-
745 latitude regions of Mars. *Journal of Geophysical Research: Planets* **112**. Available at:
746 https://agupubs.onlinelibrary.wiley.com/doi/abs/10.1029/2007JE002887 [Accessed
747 January 15, 2020].

748 Bragg M. A. and Kleeman B. Sc. (1905) XXXIX. On the α particles of radium, and their loss of
749 range in passing through various atoms and molecules. *The London, Edinburgh, and*
750 *Dublin Philosophical Magazine and Journal of Science* **10**, 318–340.

751 Broquet A. and Wieczorek M. A. (2019) The Gravitational Signature of Martian Volcanoes.
752 *Journal of Geophysical Research: Planets* **124**, 2054–2086.

753 Brounce M., Stolper E. and Eiler J. (2017) Redox variations in Mauna Kea lavas, the oxygen
754 fugacity of the Hawaiian plume, and the role of volcanic gases in Earth's oxygenation.
755 *PNAS*. Available at: https://www.pnas.org/content/early/2017/08/01/1619527114
756 [Accessed January 21, 2020].

757 Buck E. C., Wittman R. S., Skomurski F. N., Cantrell K. J., McNamara B. K. and Soderquist C. Z.
758 (2012) *Radiolysis Process Model*., Pacific Northwest National Lab. (PNNL), Richland, WA
759 (United States). Available at: https://www.osti.gov/biblio/1069211 [Accessed January
760 17, 2020].

761 Burns R. G. and Fisher D. S. (1990) Evolution of sulfide mineralization on Mars. *Journal of*
762 *Geophysical Research: Solid Earth*, 14169–14173.

763 Carter J., Viviano-Beck C., Loizeau D., Bishop J. and Le Deit L. (2015) Orbital detection and
764 implications of akaganéite on Mars. *Icarus* **253**, 296–310.

765 Cassata W. S., Cohen B. E., Mark D. F., Trappitsch R., Crow C. A., Wimpenny J., Lee M. R. and
766 Smith C. L. (2018) Chronology of martian breccia NWA 7034 and the formation of the
767 martian crustal dichotomy. *Science Advances* **4**, eaap8306.

768 Chai G. and Naldrett A. J. (1992) Characteristics of Ni-Cu-PGE mineralization and genesis of the
769 Jinchuan Deposit, Northwest China. *Economic Geology* **87**, 1475–1495.

770 Chevrier V., Lorand J.-P. and Sautter V. (2011) Sulfide petrology of four nakhlites: Northwest
771 Africa 817, Northwest Africa 998, Nakhla, and Governador Valadares. *Meteoritics &*
772 *Planetary Science* **46**, 769–784.

773 Chivian D., Brodie E. L., Alm E. J., Culley D. E., Dehal P. S., DeSantis T. Z., Gihring T. M., Lapidus
774 A., Lin L.-H., Lowry S. R., Moser D. P., Richardson P. M., Southam G., Wanger G., Pratt L.
775 M., Andersen G. L., Hazen T. C., Brockman F. J., Arkin A. P. and Onstott T. C. (2008)
776 Environmental Genomics Reveals a Single-Species Ecosystem Deep Within Earth. *Science*
777 **322**, 275–278.

778 Clark B. C., Baird A. K., Rose H. J., Toulmin P., Keil K., Castro A. J., Kelliher W. C., Rowe C. D. and
779 Evans P. H. (1976) Inorganic Analyses of Martian Surface Samples at the Viking Landing
780 Sites. *Science* **194**, 1283–1288.

781 Cockell C. S., Voytek M. A., Gronstal A. L., Finster K., Kirshtein J. D., Howard K., Reitner J., Gohn
782 G. S., Sanford W. E., Horton J. W., Kallmeyer J., Kelly L. and Powars D. S. (2012) Impact
783 Disruption and Recovery of the Deep Subsurface Biosphere. *Astrobiology* **12**, 231–246.

784 Dehouck E., Chevrier V., Gaudin A., Mangold N., Mathé P.-E. and Rochette P. (2012) Evaluating
785 the role of sulfide-weathering in the formation of sulfates or carbonates on Mars.
786 *Geochimica et Cosmochimica Acta* **90**, 47–63.

787 Desborough G. A., Anderson A. T. and Wright T. L. (1968) Mineralogy of sulfides from certain
788 Hawaiian basalts. *Economic Geology* **63**, 636–644.

789 Dickin A. P., Richardson J. M., Crocket J. H., McNutt R. H. and Peredery W. V. (1992) Osmium
790 isotope evidence for a crustal origin of platinum group elements in the Sudbury nickel
791 ore, Ontario, Canada. *Geochimica et Cosmochimica Acta* **56**, 3531–3537.

792 Ding S., Dasgupta R. and Tsuno K. (2014) Sulfur concentration of martian basalts at sulfide
793 saturation at high pressures and temperatures – Implications for deep sulfur cycle on
794 Mars. *Geochimica et Cosmochimica Acta* **131**, 227–246.

795 Dzaugis M., Spivack A. J. and D'Hondt S. (2018) Radiolytic H2 Production in Martian
796 Environments. *Astrobiology* **18**, 1137–1146.

797 Economou M. I. and Naldrett A. J. (1984) Sulfides associated with podiform bodies of chromite
798 at Tsangli, Eretria, Greece. *Mineral. Deposita* **19**, 289–297.

799 Ehlmann B. L. and Edwards C. S. (2014) Mineralogy of the Martian Surface. *Annual Review of*
800 *Earth and Planetary Sciences* **42**, 291–315.

801 Ehlmann B. L., Mustard J. F. and Murchie S. L. (2010) Geologic setting of serpentine deposits on
802 Mars. *Geophysical Research Letters* **37**. Available at:
803 https://agupubs.onlinelibrary.wiley.com/doi/abs/10.1029/2010GL042596 [Accessed
804 January 21, 2020].

805 Ehlmann B. L., Mustard J. F., Swayze G. A., Clark R. N., Bishop J. L., Poulet F., Marais D. J. D.,
806 Roach L. H., Milliken R. E., Wray J. J., Barnouin-Jha O. and Murchie S. L. (2009)
807 Identification of hydrated silicate minerals on Mars using MRO-CRISM: Geologic context
808 near Nili Fossae and implications for aqueous alteration. *Journal of Geophysical*
809 *Research: Planets* **114**. Available at:
810 https://agupubs.onlinelibrary.wiley.com/doi/abs/10.1029/2009JE003339 [Accessed
811 April 8, 2019].

812 Evans-Lamswood D. M., Butt D. P., Jackson R. S., Lee D. V., Muggridge M. G., Wheeler R. I. and
813 Wilton D. H. C. (2000) Physical Controls Associated with the Distribution of Sulfides in
814 the Voisey's Bay Ni-Cu-Co Deposit, Labrador. *Economic Geology* **95**, 749–769.

815 Foley C. N., Economou T. and Clayton R. N. (2003) Final chemical results from the Mars
816 Pathfinder alpha proton X-ray spectrometer. *Journal of Geophysical Research: Planets*
817 **108**. Available at:
818 https://agupubs.onlinelibrary.wiley.com/doi/abs/10.1029/2002JE002019 [Accessed July
819 9, 2020].

820 Franz H. B., Kim S.-T., Farquhar J., Day J. M. D., Economos R. C., McKeegan K. D., Schmitt A. K.,
821 Irving A. J., Hoek J. and Iii J. D. (2014) Isotopic links between atmospheric chemistry and
822 the deep sulphur cycle on Mars. *Nature* **508**, 364–368.

823 Franz H. B., McAdam A. C., Ming D. W., Freissinet C., Mahaffy P. R., Eldridge D. L., Fischer W. W.,
824 Grotzinger J. P., House C. H., Hurowitz J. A., McLennan S. M., Schwenzer S. P., Vaniman
825 D. T., Archer Jr P. D., Atreya S. K., Conrad P. G., Dottin Iii J. W., Eigenbrode J. L., Farley K.
826 A., Glavin D. P., Johnson S. S., Knudson C. A., Morris R. V., Navarro-González R., Pavlov A.
827 A., Plummer R., Rampe E. B., Stern J. C., Steele A., Summons R. E. and Sutter B. (2017)
828 Large sulfur isotope fractionations in Martian sediments at Gale crater. *Nature*
829 *Geoscience* **10**, 658–662.

830 Franz H. B., Wu N., Farquhar J. and Irving A. J. (2019) A new type of isotopic anomaly in
831 shergottite sulfides. *Meteoritics & Planetary Science* **54**, 3036–3051.

832 Fuller E. R. and Head J. W. (2003) Olympus Mons, Mars: Detection of extensive preaureole
833 volcanism and implications for initial mantle plume behavior. *Geology* **31**, 175–178.

834 Gain S. B. and Mostert A. B. (1982) The geological setting of the platinoid and base metal sulfide
835 mineralization in the Platreef of the Bushveld Complex in Drenthe, North of
836 Potgietersrus. *Economic Geology* **77**, 1395–1404.

837 Gattacceca J., Hewins R. H., Lorand J.-P., Rochette P., Lagroix F., Cournède C., Uehara M., Pont
838 S., Sautter V., Scorzelli R. B., Hombourger C., Munayco P., Zanda B., Chennaoui H. and
839 Ferrière L. (2013) Opaque minerals, magnetic properties, and paleomagnetism of the
840 Tissint Martian meteorite. *Meteoritics & Planetary Science* **48**, 1919–1936.

841 Gellert R., Rieder R., Anderson R. C., Brückner J., Clark B. C., Dreibus G., Economou T.,
842 Klingelhöfer G., Lugmair G. W., Ming D. W., Squyres S. W., d'Uston C., Wänke H., Yen A.
843 and Zipfel J. (2004) Chemistry of Rocks and Soils in Gusev Crater from the Alpha Particle
844 X-ray Spectrometer. *Science* **305**, 829–832.

845 Goossens S., Sabaka T. J., Genova A., Mazarico E., Nicholas J. B. and Neumann G. A. (2017)
846 Evidence for a low bulk crustal density for Mars from gravity and topography.
847 *Geophysical Research Letters* **44**, 7686–7694.

Greenwood J. P., Mojzsis S. J. and Coath C. D. (2000a) Sulfur isotopic compositions of individual sulfides in Martian meteorites ALH84001 and Nakhla: implications for crust–regolith exchange on Mars. *Earth and Planetary Science Letters* **184**, 23–35.

Greenwood J. P., Riciputi L. R., McSween H. Y. and Taylor L. A. (2000b) Modified sulfur isotopic compositions of sulfides in the nakhlites and Chassigny. *Geochimica et Cosmochimica Acta* **64**, 1121–1131.

Grimm R. E., Harrison K. P., Stillman D. E. and Kirchoff M. R. (2017) On the secular retention of ground water and ice on Mars. *Journal of Geophysical Research: Planets* **122**, 94–109.

Hahn B. C., McLennan S. M. and Klein E. C. (2011) Martian surface heat production and crustal heat flow from Mars Odyssey Gamma-Ray spectrometry. *Geophysical Research Letters* **38**. Available at: https://agupubs.onlinelibrary.wiley.com/doi/abs/10.1029/2011GL047435 [Accessed January 21, 2020].

Herd C. D. K. (2003) The oxygen fugacity of olivine-phyric martian basalts and the components within the mantle and crust of Mars. *Meteoritics & Planetary Science* **38**, 1793–1805.

Hewins R. H., Humayun M., Barrat J.-A., Zanda B., Lorand J.-P., Pont S., Assayag N., Cartigny P., Yang S. and Sautter V. (2020) Northwest Africa 8694, a ferroan chassignite: Bridging the gap between nakhlites and chassignites. *Geochimica et Cosmochimica Acta* **282**, 201–226.

Hewins R. H., Zanda B., Humayun M., Nemchin A., Lorand J.-P., Pont S., Deldicque D., Bellucci J. J., Beck P., Leroux H., Marinova M., Remusat L., Göpel C., Lewin E., Grange M., Kennedy A. and Whitehouse M. J. (2017) Regolith breccia Northwest Africa 7533: Mineralogy and petrology with implications for early Mars. *Meteoritics & Planetary Science* **52**, 89–124.

Holland G., Lollar B. S., Li L., Lacrampe-Couloume G., Slater G. F. and Ballentine C. J. (2013) Deep fracture fluids isolated in the crust since the Precambrian era. *Nature* **497**, 357–360.

Humayun M., Yang S., Irving A. J. and Righter K. (2019) Sulfide Assimilation and Mineralization in Ancient (2.4 Ga) Shergottites. **2157**, 6380.

Hynek B. M., Robbins S. J., Šrámek O. and Zhong S. J. (2011) Geological evidence for a migrating Tharsis plume on early Mars. *Earth and Planetary Science Letters* **310**, 327–333.

Johnson C. L., Mittelholz A., Langlais B., Russell C. T., Ansan V., Banfield D., Chi P. J., Fillingim M. O., Forget F., Haviland H. F., Golombek M., Joy S., Lognonné P., Liu X., Michaut C., Pan L., Quantin-Nataf C., Spiga A., Stanley S., Thorne S. N., Wieczorek M. A., Yu Y., Smrekar S. E. and Banerdt W. B. (2020) Crustal and time-varying magnetic fields at the InSight landing site on Mars. *Nature Geoscience* **13**, 199–204.

King P. L. and McSween H. Y. (2005) Effects of H2O, pH, and oxidation state on the stability of Fe minerals on Mars. *Journal of Geophysical Research: Planets* **110**. Available at: https://agupubs.onlinelibrary.wiley.com/doi/abs/10.1029/2005JE002482 [Accessed July 9, 2020].

Klein F., Tarnas J. D. and Bach W. (2020) Abiotic Sources of Molecular Hydrogen on Earth. *Elements* **16**, 19–24.

Kremer C. H., Mustard J. F. and Bramble M. S. (2019) A widespread olivine-rich ash deposit on Mars. *Geology* **47**, 677–681.

Kumagai Y., Kimura A., Taguchi M., Nagaishi R., Yamagishi I. and Kimura T. (2013) Hydrogen production in gamma radiolysis of the mixture of mordenite and seawater. *Journal of Nuclear Science and Technology* **50**, 130–138.

Langlais B., Thébault E., Houliez A., Purucker M. E. and Lillis R. J. (2019) A New Model of the Crustal Magnetic Field of Mars Using MGS and MAVEN. *Journal of Geophysical Research: Planets* **124**, 1542–1569.

LaVerne J. A. and Tandon L. (2005) H2 and Cl2 Production in the Radiolysis of Calcium and Magnesium Chlorides and Hydroxides. *J. Phys. Chem. A* **109**, 2861–2865.

Le Deit L., Mangold N., Forni O., Cousin A., Lasue J., Schröder S., Wiens R. C., Sumner D., Fabre C., Stack K. M., Anderson R. B., Blaney D., Clegg S., Dromart G., Fisk M., Gasnault O., Grotzinger J. P., Gupta S., Lanza N., Mouélic S. L., Maurice S., McLennan S. M., Meslin P.-Y., Nachon M., Newsom H., Payré V., Rapin W., Rice M., Sautter V. and Treiman A. H. (2016) The potassic sedimentary rocks in Gale Crater, Mars, as seen by ChemCam on board Curiosity. *Journal of Geophysical Research: Planets* **121**, 784–804.

Leask E. K., Ehlmann B. L., Dundar M. M., Murchie S. L. and Seelos F. P. (2018) Challenges in the Search for Perchlorate and Other Hydrated Minerals With 2.1-µm Absorptions on Mars. *Geophysical Research Letters* **45**, 12,180-12,189.

Lefticariu L., Pratt L. A., LaVerne J. A. and Schimmelmann A. (2010) Anoxic pyrite oxidation by water radiolysis products — A potential source of biosustaining energy. *Earth and Planetary Science Letters* **292**, 57–67.

Lewis K. W., Peters S., Gonter K., Morrison S., Schmerr N., Vasavada A. R. and Gabriel T. (2019) A surface gravity traverse on Mars indicates low bedrock density at Gale crater. *Science* **363**, 535–537.

Li L., Wing B. A., Bui T. H., McDermott J. M., Slater G. F., Wei S., Lacrampe-Couloume G. and Lollar B. S. (2016) Sulfur mass-independent fractionation in subsurface fracture waters indicates a long-standing sulfur cycle in Precambrian rocks. *Nat Commun* **7**, 1–9.

916 Lightfoot P. C. and Evans-Lamswood D. (2015) Structural controls on the primary distribution of
917 mafic–ultramafic intrusions containing Ni–Cu–Co–(PGE) sulfide mineralization in the
918 roots of large igneous provinces. *Ore Geology Reviews* **64**, 354–386.

919 Lin L.-H., Hall J., Lippmann-Pipke J., Ward J. A., Lollar B. S., DeFlaun M., Rothmel R., Moser D.,
920 Gihring T. M., Mislowack B. and Onstott T. C. (2005a) Radiolytic H2 in continental crust:
921 Nuclear power for deep subsurface microbial communities. *Geochemistry, Geophysics,*
922 *Geosystems* **6**. Available at:
923 https://agupubs.onlinelibrary.wiley.com/doi/abs/10.1029/2004GC000907 [Accessed
924 January 6, 2020].

925 Lin L.-H., Slater G. F., Sherwood Lollar B., Lacrampe-Couloume G. and Onstott T. C. (2005b) The
926 yield and isotopic composition of radiolytic H2, a potential energy source for the deep
927 subsurface biosphere. *Geochimica et Cosmochimica Acta* **69**, 893–903.

928 Lin L.-H., Wang P.-L., Rumble D., Lippmann-Pipke J., Boice E., Pratt L. M., Lollar B. S., Brodie E. L.,
929 Hazen T. C., Andersen G. L., DeSantis T. Z., Moser D. P., Kershaw D. and Onstott T. C.
930 (2006) Long-Term Sustainability of a High-Energy, Low-Diversity Crustal Biome. *Science*
931 **314**, 479–482.

932 Lollar G. S., Warr O., Telling J., Osburn M. R. and Lollar B. S. (2019) 'Follow the Water':
933 Hydrogeochemical Constraints on Microbial Investigations 2.4 km Below Surface at the
934 Kidd Creek Deep Fluid and Deep Life Observatory. *Geomicrobiology Journal* **36**, 859–872.

935 Lorand J.-P. (1985) The behaviour of the upper mantle sulfide component during the incipient
936 alteration of "Alpine"-type peridotites as illustrated by the Beni Bousera (northern
937 Morocco) and Ronda (southern Spain) ultramafic bodies. *TMPM Tschermaks Petr. Mitt.*
938 **34**, 183–209.

939 Lorand J.-P., Barrat J.-A., Chevrier V., Sautter V. and Pont S. (2012) Metal-saturated sulfide
940 assemblages in NWA 2737: Evidence for impact-related sulfur devolatilization in Martian
941 meteorites. *Meteoritics & Planetary Science* **47**, 1830–1841.

942 Lorand J.-P., Chevrier V. and Sautter V. (2005) Sulfide mineralogy and redox conditions in some
943 shergottites. *Meteoritics & Planetary Science* **40**, 1257–1272.

944 Lorand J.-P., Hewins R. H., Humayun M., Remusat L., Zanda B., La C. and Pont S. (2018a)
945 Chalcophile-siderophile element systematics of hydrothermal pyrite from martian
946 regolith breccia NWA 7533. *Geochimica et Cosmochimica Acta* **241**, 134–149.

947 Lorand J.-P., Hewins R. H., Remusat L., Zanda B., Pont S., Leroux H., Marinova M., Jacob D.,
948 Humayun M., Nemchin A., Grange M., Kennedy A. and Göpel C. (2015) Nickeliferous
949 pyrite tracks pervasive hydrothermal alteration in Martian regolith breccia: A study in
950 NWA 7533. *Meteoritics & Planetary Science* **50**, 2099–2120.

951 Lorand J.-P., Pont S., Chevrier V., Luguet A., Zanda B. and Hewins R. (2018b) Petrogenesis of
952 martian sulfides in the Chassigny meteorite. *American Mineralogist* **103**, 872–885.

953 Magnabosco C., Lin L.-H., Dong H., Bomberg M., Ghiorse W., Stan-Lotter H., Pedersen K., Kieft T.
954 L., van Heerden E. and Onstott T. C. (2018) The biomass and biodiversity of the
955 continental subsurface. *Nature Geoscience* **11**, 707–717.

956 Mari N., Riches A. J. V., Hallis L. J., Marrocchi Y., Villeneuve J., Gleissner P., Becker H. and Lee M.
957 R. (2019) Syneruptive incorporation of martian surface sulphur in the nakhlite lava flows
958 revealed by S and Os isotopes and highly siderophile elements: implication for mantle
959 sources in Mars. *Geochimica et Cosmochimica Acta* **266**, 416–434.

960 Marques A. F. A., Barriga F. J. A. S. and Scott S. D. (2007) Sulfide mineralization in an ultramafic-
961 rock hosted seafloor hydrothermal system: From serpentinization to the formation of
962 Cu–Zn–(Co)-rich massive sulfides. *Marine Geology* **245**, 20–39.

963 Martin P. E., Farley K. A., Baker M. B., Malespin C. A., Schwenzer S. P., Cohen B. A., Mahaffy P.
964 R., McAdam A. C., Ming D. W., Vasconcelos P. M. and Navarro-González R. (2017) A Two-
965 Step K-Ar Experiment on Mars: Dating the Diagenetic Formation of Jarosite from
966 Amazonian Groundwaters. *Journal of Geophysical Research: Planets* **122**, 2803–2818.

967 McAdam A. C., Franz H. B., Sutter B., Archer P. D., Freissinet C., Eigenbrode J. L., Ming D. W.,
968 Atreya S. K., Bish D. L., Blake D. F., Bower H. E., Brunner A., Buch A., Glavin D. P.,
969 Grotzinger J. P., Mahaffy P. R., McLennan S. M., Morris R. V., Navarro-González R.,
970 Rampe E. B., Squyres S. W., Steele A., Stern J. C., Sumner D. Y. and Wray J. J. (2014)
971 Sulfur-bearing phases detected by evolved gas analysis of the Rocknest aeolian deposit,
972 Gale Crater, Mars. *Journal of Geophysical Research: Planets* **119**, 373–393.

973 McDonough W. F. and Sun S. (1995) The composition of the Earth. *Chemical Geology* **120**, 223–
974 253.

975 McLennan S. M., Bell J. F., Calvin W. M., Christensen P. R., Clark B. C., de Souza P. A., Farmer J.,
976 Farrand W. H., Fike D. A., Gellert R., Ghosh A., Glotch T. D., Grotzinger J. P., Hahn B.,
977 Herkenhoff K. E., Hurowitz J. A., Johnson J. R., Johnson S. S., Jolliff B., Klingelhöfer G.,
978 Knoll A. H., Learner Z., Malin M. C., McSween H. Y., Pocock J., Ruff S. W., Soderblom L.
979 A., Squyres S. W., Tosca N. J., Watters W. A., Wyatt M. B. and Yen A. (2005) Provenance
980 and diagenesis of the evaporite-bearing Burns formation, Meridiani Planum, Mars. *Earth*
981 *and Planetary Science Letters* **240**, 95–121.

982 McLennan S. M., Boynton W. V., Karunatillake S., Hahn B. C., Taylor G. J. and Mars Odyssey GRS
983 Team (2010) Distribution of Sulfur on the Surface of Mars Determined by the 2001 Mars
984 Odyssey Gamma Ray Spectrometer. **41**, 2174.

985 McMahon S., Parnell J., Ponicka J., Hole M. and Boyce A. (2013) The habitability of vesicles in
986 martian basaltMars habitability. *A&G* **54**, 1.17-1.21.

McSween H. Y. (2015) Petrology on Mars. *American Mineralogist* **100**, 2380–2395.

Meyer C. (2016) The Martian Meteorite Compendium.

Michalski J. R., Cuadros J., Niles P. B., Parnell J., Rogers A. D. and Wright S. P. (2013) Groundwater activity on Mars and implications for a deep biosphere. *Nature Geosci* **6**, 133–138.

Michalski J. R., Dobrea E. Z. N., Niles P. B. and Cuadros J. (2017) Ancient hydrothermal seafloor deposits in Eridania basin on Mars. *Nature Communications* **8**, 15978.

Michalski J. R., Onstott T. C., Mojzsis S. J., Mustard J., Chan Q. H. S., Niles P. B. and Johnson S. S. (2018) The Martian subsurface as a potential window into the origin of life. *Nature Geoscience* **11**, 21–26.

Morris R. V., Ruff S. W., Gellert R., Ming D. W., Arvidson R. E., Clark B. C., Golden D. C., Siebach K., Klingelhöfer G., Schröder C., Fleischer I., Yen A. S. and Squyres S. W. (2010) Identification of Carbonate-Rich Outcrops on Mars by the Spirit Rover. *Science* **329**, 421–424.

Morrison S. M., Downs R. T., Blake D. F., Vaniman D. T., Ming D. W., Hazen R. M., Treiman A. H., Achilles C. N., Yen A. S., Morris R. V., Rampe E. B., Bristow T. F., Chipera S. J., Sarrazin P. C., Gellert R., Fendrich K. V., Morookian J. M., Farmer J. D., Marais D. J. D. and Craig P. I. (2018) Crystal chemistry of martian minerals from Bradbury Landing through Naukluft Plateau, Gale crater, Mars. *American Mineralogist* **103**, 857–871.

Mungall J. E., Ames D. E. and Hanley J. J. (2004) Geochemical evidence from the Sudbury structure for crustal redistribution by large bolide impacts. *Nature* **429**, 546–548.

Nambu M. (1968) New mineral Akaganeite, β-FeOOH, from Akagane Mine, Iwate Prefecture, Japan. *The Journal of the Japanese Association of Mineralogists, Petrologists and Economic Geologists* **59**, 143–151.

National Academies of Sciences, Engineering, and Medicine, Division on Engineering and Physical Sciences, Space Studies Board and Committee on Astrobiology Science Strategy for the Search for Life in the Universe (2018) *An Astrobiology Strategy for the Search for Life in the Universe*., National Academies Press (US), Washington (DC). Available at: http://www.ncbi.nlm.nih.gov/books/NBK540091/ [Accessed July 23, 2020].

Nogami H. H. and Hurley P. M. (1948) The absorption factor in counting alpha rays from thick mineral sources. *Eos, Transactions American Geophysical Union* **29**, 335–340.

Onstott, T.C., McGown D., Kessler J., Lollar B. S., Lehmann K. K. and Clifford S. M. (2006) Martian CH4: Sources, Flux, and Detection. *Astrobiology* **6**, 377–395.

Onstott T. C., Ehlmann B. l., Sapers H., Coleman M., Ivarsson M., Marlow J. J., Neubeck A. and Niles P. (2019) Paleo-Rock-Hosted Life on Earth and the Search on Mars: A Review and Strategy for Exploration. *Astrobiology* **19**, 1230–1262.

Onstott T. C., Moser D. P., Pfiffner S. M., Fredrickson J. K., Brockman F. J., Phelps T. J., White D. C., Peacock A., Balkwill D., Hoover R., Krumholz L. R., Borscik M., Kieft T. L. and Wilson R. (2003) Indigenous and contaminant microbes in ultradeep mines. *Environmental Microbiology* **5**, 1168–1191.

Payré V., Fabre C., Sautter V., Cousin A., Mangold N., Deit L. L., Forni O., Goetz W., Wiens R. C., Gasnault O., Meslin P.-Y., Lasue J., Rapin W., Clark B., Nachon M., Lanza N. L. and Maurice S. (2019) Copper enrichments in the Kimberley formation in Gale crater, Mars: Evidence for a Cu deposit at the source. *Icarus* **321**, 736–751.

Rampe E. B., Ming D. W., Blake D. F., Bristow T. F., Chipera S. J., Grotzinger J. P., Morris R. V., Morrison S. M., Vaniman D. T., Yen A. S., Achilles C. N., Craig P. I., Des Marais D. J., Downs R. T., Farmer J. D., Fendrich K. V., Gellert R., Hazen R. M., Kah L. C., Morookian J. M., Peretyazhko T. S., Sarrazin P., Treiman A. H., Berger J. A., Eigenbrode J., Fairén A. G., Forni O., Gupta S., Hurowitz J. A., Lanza N. L., Schmidt M. E., Siebach K., Sutter B. and Thompson L. M. (2017) Mineralogy of an ancient lacustrine mudstone succession from the Murray formation, Gale crater, Mars. *Earth and Planetary Science Letters* **471**, 172–185.

Redmond H. L. and King S. D. (2004) A numerical study of a mantle plume beneath the Tharsis Rise: Reconciling dynamic uplift and lithospheric support models. *Journal of Geophysical Research: Planets* **109**. Available at: https://agupubs.onlinelibrary.wiley.com/doi/abs/10.1029/2003JE002228 [Accessed July 9, 2020].

Rochette P., Gattacceca J., Chevrier V., Hoffmann V., Lorand J.-P., Funaki M. and Hochleitner R. (2005) Matching Martian crustal magnetization and magnetic properties of Martian meteorites. *Meteoritics & Planetary Science* **40**, 529–540.

Rochette P., Lorand J.-P., Fillion G. and Sautter V. (2001) Pyrrhotite and the remanent magnetization of SNC meteorites: a changing perspective on Martian magnetism. *Earth and Planetary Science Letters* **190**, 1–12.

Ruff S. W. (2004) Spectral evidence for zeolite in the dust on Mars. *Icarus* **168**, 131–143.

Ruff S. W., Campbell K. A., Van Kranendonk M. J., Rice M. S. and Farmer J. D. (2019) The Case for Ancient Hot Springs in Gusev Crater, Mars. *Astrobiology* **20**, 475–499.

Ruff S. W. and Farmer J. D. (2016) Silica deposits on Mars with features resembling hot spring biosignatures at El Tatio in Chile. *Nature Communications* **7**, 13554.

Ruff S. W., Farmer J. D., Calvin W. M., Herkenhoff K. E., Johnson J. R., Morris R. V., Rice M. S., Arvidson R. E., Bell III J. F., Christensen P. R. and Squyres S. W. (2011) Characteristics, distribution, origin, and significance of opaline silica observed by the Spirit rover in Gusev crater, Mars. *Journal of Geophysical Research: Planets* **116**. Available at: https://agupubs.onlinelibrary.wiley.com/doi/10.1029/2010JE003767 [Accessed April 8, 2019].

Ruff S. W., Hamilton V. E., Rogers A. D., Edwards C. S. and Horgan B. (2019) Olivine-Rich, Carbonate-Bearing Ash Deposits Link Jezero and Gusev Craters. **50**, 2775.

Ruff S. W., Niles P. B., Alfano F. and Clarke A. B. (2014) Evidence for a Noachian-aged ephemeral lake in Gusev crater, Mars. *Geology* **42**, 359–362.

Schwenzer S. P., Abramov O., Allen C. C., Clifford S. M., Cockell C. S., Filiberto J., Kring D. A., Lasue J., McGovern P. J., Newsom H. E., Treiman A. H., Vaniman D. T. and Wiens R. C. (2012) Puncturing Mars: How impact craters interact with the Martian cryosphere. *Earth and Planetary Science Letters* **335–336**, 9–17.

Sheppard R. Y., Milliken R. E., Itoh Y. and Parente M. (2019) Mineral Stratigraphy Around Mt. Sharp Suggests Aqueous Processes Affected the Entire Mound: Directions for Upcoming Rover Observations from Orbital Data. *LPI Contributions* **2089**, 6289.

Sherwood Lollar B., Voglesonger K., Lin L.-H., Lacrampe-Couloume G., Telling J., Abrajano T. a., Onstott T. c. and Pratt L. m. (2007) Hydrogeologic Controls on Episodic H2 Release from Precambrian Fractured Rocks—Energy for Deep Subsurface Life on Earth and Mars. *Astrobiology* **7**, 971–986.

Sherwood Lollar B., Onstott T. C., Lacrampe-Couloume G. and Ballentine C. J. (2014) The contribution of the Precambrian continental lithosphere to global H 2 production. *Nature* **516**, 379–382.

Shiga Y. (1987) Behavior of iron, nickel, cobalt and sulfur during serpentinization, with reference to the Hayachine ultramafic rocks of the Kamaishi mining district, northeastern Japan.

Sleep N. H. (2012) Maintenance of permeable habitable subsurface environments by earthquakes and tidal stresses. *International Journal of Astrobiology* **11**, 257–268.

Sleep N. H., Meibom A., Fridriksson T., Coleman R. G. and Bird D. K. (2004) H2-rich fluids from serpentinization: Geochemical and biotic implications. *PNAS* **101**, 12818–12823.

Squyres S. W., Arvidson R. E., Bell J. F., Calef F., Clark B. C., Cohen B. A., Crumpler L. A., Souza P. A. de, Farrand W. H., Gellert R., Grant J., Herkenhoff K. E., Hurowitz J. A., Johnson J. R., Jolliff B. L., Knoll A. H., Li R., McLennan S. M., Ming D. W., Mittlefehldt D. W., Parker T. J., Paulsen G., Rice M. S., Ruff S. W., Schröder C., Yen A. S. and Zacny K. (2012) Ancient Impact and Aqueous Processes at Endeavour Crater, Mars. *Science* **336**, 570–576.

Squyres S. W., Arvidson R. E., Ruff S., Gellert R., Morris R. V., Ming D. W., Crumpler L., Farmer J. D., Marais D. J. D., Yen A., McLennan S. M., Calvin W., Bell J. F., Clark B. C., Wang A., McCoy T. J., Schmidt M. E. and Souza P. A. de (2008) Detection of Silica-Rich Deposits on Mars. *Science* **320**, 1063–1067.

Stamenković V., Beegle L. W., Zacny K., Arumugam D. D., Baglioni P., Barba N., Baross J., Bell M. S., Bhartia R., Blank J. G., Boston P. J., Breuer D., Brinckerhoff W., Burgin M. S., Cooper I., Cormarkovic V., Davila A., Davis R. M., Edwards C., Etiope G., Fischer W. W., Glavin D. P., Grimm R. E., Inagaki F., Kirschvink J. L., Kobayashi A., Komarek T., Malaska M., Michalski J., Ménez B., Mischna M., Moser D., Mustard J., Onstott T. C., Orphan V. J., Osburn M. R., Plaut J., Plesa A.-C., Putzig N., Rogers K. L., Rothschild L., Russell M., Sapers H., Lollar B. S., Spohn T., Tarnas J. D., Tuite M., Viola D., Ward L. M., Wilcox B. and Woolley R. (2019) The next frontier for planetary and human exploration. *Nature Astronomy* **3**, 116–120.

Stamenković V., Ward L. M., Mischna M. and Fischer W. W. (2018) O 2 solubility in Martian near-surface environments and implications for aerobic life. *Nature Geoscience* **11**, 905–909.

Stanley B. D., Hirschmann M. M. and Withers A. C. (2011) CO2 solubility in Martian basalts and Martian atmospheric evolution. *Geochimica et Cosmochimica Acta* **75**, 5987–6003.

Tarnas J. D., Mustard J. F., Sherwood Lollar B., Bramble M. S., Cannon K. M., Palumbo A. M. and Plesa A.-C. (2018) Radiolytic H2 production on Noachian Mars: Implications for habitability and atmospheric warming. *Earth and Planetary Science Letters* **502**, 133–145.

Thalhammer O., Stumpfl E. F. and Panayiotou A. (1986) Postmagmatic, hydrothermal origin of sulfide and arsenide mineralizations at Limassol Forest, Cyprus. *Mineral. Deposita* **21**, 95–105.

Therriault A. M., Fowler A. D. and Grieve R. A. F. (2002) The Sudbury Igneous Complex: A Differentiated Impact Melt Sheet. *Economic Geology* **97**, 1521–1540.

Vaniman D. T., Bish D. L., Ming D. W., Bristow T. F., Morris R. V., Blake D. F., Chipera S. J., Morrison S. M., Treiman A. H., Rampe E. B., Rice M., Achilles C. N., Grotzinger J. P., McLennan S. M., Williams J., Bell J. F., Newsom H. E., Downs R. T., Maurice S., Sarrazin P., Yen A. S., Morookian J. M., Farmer J. D., Stack K., Milliken R. E., Ehlmann B. L., Sumner D. Y., Berger G., Crisp J. A., Hurowitz J. A., Anderson R., Marais D. J. D., Stolper E. M., Edgett K. S., Gupta S., Spanovich N. and Team M. S. (2014) Mineralogy of a Mudstone at Yellowknife Bay, Gale Crater, Mars. *Science* **343**. Available at: https://science.sciencemag.org/content/343/6169/1243480 [Accessed January 15, 2020].

Wafik A., Admou H., Saquaque A., Boukhari A. E. and Juteau T. (2001) Les Minéralisations Sulfurées à Cu-Fe et les Altérations Associées dans les Ophiolites Protérozoiques de Bou Azzer et de Khzama (Anti-Atlas, Maroc) (Cu-Fe sulfureous mineralisations and the associated alterations in the Bou Azzer and Khzama Proterozoic ophiolites, Anti-Atlas, Maroc). *Ofioliti* **26**, 47–62.

Walker R. J., Morgan J. W., Naldrett A. J., Li C. and Fassett J. D. (1991) Re-Os isotope systematics of Ni-Cu sulfide ores, Sudbury Igneous Complex, Ontario: evidence for a major crustal component. *Earth and Planetary Science Letters* **105**, 416–429.

Wang Z. and Becker H. (2017) Chalcophile elements in Martian meteorites indicate low sulfur content in the Martian interior and a volatile element-depleted late veneer. *Earth and Planetary Science Letters* **463**, 56–68.

Warr O., Giunta T., Ballentine C. J. and Sherwood Lollar B. (2019) Mechanisms and rates of 4He, 40Ar, and H2 production and accumulation in fracture fluids in Precambrian Shield environments. *Chemical Geology* **530**, 119322.

Warr O., Sherwood Lollar B., Fellowes J., Sutcliffe C. N., McDermott J. M., Holland G., Mabry J. C. and Ballentine C. J. (2018) Tracing ancient hydrogeological fracture network age and compartmentalisation using noble gases. *Geochimica et Cosmochimica Acta* **222**, 340–362.

Weiss B. P., Yung Y. L. and Nealson K. H. (2000) Atmospheric energy for subsurface life on Mars? *PNAS* **97**, 1395–1399.

West M. D. and Clarke J. D. A. (2010) Potential martian mineral resources: Mechanisms and terrestrial analogues. *Planetary and Space Science* **58**, 574–582.

Whitney J. A. (1984) Fugacities of sulfurous gases in pyrrhotite-bearing silicic magmas. *American Mineralogist* **69**, 68–78.

Wiseman S. M., Arvidson R. E., Andrews-Hanna J. C., Clark R. N., Lanza N. L., Marais D. D., Marzo G. A., Morris R. V., Murchie S. L., Newsom H. E., Dobrea E. Z. N., Ollila A. M., Poulet F., Roush T. L., Seelos F. P. and Swayze G. A. (2008) Phyllosilicate and sulfate-hematite deposits within Miyamoto crater in southern Sinus Meridiani, Mars. *Geophysical Research Letters* **35**. Available at: https://agupubs.onlinelibrary.wiley.com/doi/abs/10.1029/2008GL035363 [Accessed March 25, 2020].

Wittmann A., Korotev R. L., Jolliff B. L., Irving A. J., Moser D. E., Barker I. and Rumble D. (2015) Petrography and composition of Martian regolith breccia meteorite Northwest Africa 7475. *Meteoritics & Planetary Science* **50**, 326–352.

Wong G. M., Lewis J. M. T., Knudson C. A., Millan M., McAdam A. C., Eigenbrode J. L., Andrejkovičová S., Gómez F., Navarro-González R. and House C. H. (2020) Detection of

reduced sulfur on Vera Rubin ridge by quadratic discriminant analysis of volatiles observed during evolved gas analysis. *Journal of Geophysical Research: Planets* **n/a**, e2019JE006304.

Yen A. S., Ming D. W., Vaniman D. T., Gellert R., Blake D. F., Morris R. V., Morrison S. M., Bristow T. F., Chipera S. J., Edgett K. S., Treiman A. H., Clark B. C., Downs R. T., Farmer J. D., Grotzinger J. P., Rampe E. B., Schmidt M. E., Sutter B. and Thompson L. M. (2017) Multiple stages of aqueous alteration along fractures in mudstone and sandstone strata in Gale Crater, Mars. *Earth and Planetary Science Letters* **471**, 186–198.

Zieg M. J. and Marsh B. D. (2005) The Sudbury Igneous Complex: Viscous emulsion differentiation of a superheated impact melt sheet. *GSA Bulletin* **117**, 1427–1450.

Zolotov M. Y. and Shock E. L. (2005) Formation of jarosite-bearing deposits through aqueous oxidation of pyrite at Meridiani Planum, Mars. *Geophysical Research Letters* **32**. Available at: https://agupubs.onlinelibrary.wiley.com/doi/abs/10.1029/2005GL024253 [Accessed January 21, 2020].